

<b>Title</b>	Kinetics and coverage dependent reaction mechanisms of the copper atomic layer deposition from copper dimethylamino-2-propoxide and diethylzinc
<b>Author(s)</b>	Maimaiti, Yasheng; Elliott, Simon D.
<b>Publication date</b>	2016-08-11
<b>Original citation</b>	Maimaiti, Yasheng; Elliott, Simon D. (2016) 'Kinetics and coverage dependent reaction mechanisms of the copper atomic layer deposition from copper dimethylamino-2-propoxide and diethylzinc'. Chemistry Materials, 28 (17) :6282-6295. doi: 10.1021/acs.chemmater.6b02522
<b>Type of publication</b>	Article (peer-reviewed)
<b>Link to publisher's version</b>	<a href="http://pubs.acs.org/doi/abs/10.1021/acs.chemmater.6b02522">http://pubs.acs.org/doi/abs/10.1021/acs.chemmater.6b02522</a> <a href="http://dx.doi.org/10.1021/acs.chemmater.6b02522">http://dx.doi.org/10.1021/acs.chemmater.6b02522</a> Access to the full text of the published version may require a subscription.
<b>Rights</b>	<b>This document is the Accepted Manuscript version of a Published Work that appeared in final form in Chemistry Materials, copyright © American Chemical Society after peer review and technical editing by the publisher. To access the final edited and published work see</b> <a href="http://pubs.acs.org/doi/abs/10.1021/acs.chemmater.6b02522">http://pubs.acs.org/doi/abs/10.1021/acs.chemmater.6b02522</a>
<b>Embargo information</b>	Access to this article is restricted until 12 months after publication by the request of the publisher.
<b>Embargo lift date</b>	2017-08-11
<b>Item downloaded from</b>	<a href="http://hdl.handle.net/10468/3236">http://hdl.handle.net/10468/3236</a>

Downloaded on 2018-08-23T18:38:36Z

## Article

# Kinetics and Coverage Dependent Reaction Mechanisms of the Copper Atomic Layer Deposition from Copper Dimethylamino-2-propoxide and Diethylzinc

Yasheng Maimaiti, and Simon D Elliott

*Chem. Mater.*, **Just Accepted Manuscript** • DOI: 10.1021/acs.chemmater.6b02522 • Publication Date (Web): 11 Aug 2016Downloaded from <http://pubs.acs.org> on August 16, 2016

## Just Accepted

“Just Accepted” manuscripts have been peer-reviewed and accepted for publication. They are posted online prior to technical editing, formatting for publication and author proofing. The American Chemical Society provides “Just Accepted” as a free service to the research community to expedite the dissemination of scientific material as soon as possible after acceptance. “Just Accepted” manuscripts appear in full in PDF format accompanied by an HTML abstract. “Just Accepted” manuscripts have been fully peer reviewed, but should not be considered the official version of record. They are accessible to all readers and citable by the Digital Object Identifier (DOI®). “Just Accepted” is an optional service offered to authors. Therefore, the “Just Accepted” Web site may not include all articles that will be published in the journal. After a manuscript is technically edited and formatted, it will be removed from the “Just Accepted” Web site and published as an ASAP article. Note that technical editing may introduce minor changes to the manuscript text and/or graphics which could affect content, and all legal disclaimers and ethical guidelines that apply to the journal pertain. ACS cannot be held responsible for errors or consequences arising from the use of information contained in these “Just Accepted” manuscripts.

1  
2  
3  
4  
5  
6  
7 Kinetics and Coverage Dependent Reaction  
8  
9  
10  
11 Mechanisms of the Copper Atomic Layer  
12  
13  
14  
15 Deposition from Copper Dimethylamino-2-  
16  
17  
18  
19  
20 propoxide and Diethylzinc  
21  
22  
23  
24

25 *Yasheng Maimaiti and Simon D. Elliott\**  
26  
27

28 Tyndall National Institute, University College Cork, Lee Maltings, Prospect Row, Cork, Ireland  
29  
30  
31

32 ABSTRACT: Atomic layer deposition (ALD) has been recognized as a promising method to  
33 deposit conformal and uniform thin film of copper for future electronic devices. However, many  
34 aspects of the reaction mechanism and the surface chemistry of copper ALD remain unclear. In  
35 this paper, we employ plane wave density functional theory (DFT) to study the transmetalation  
36 ALD reaction of copper dimethylamino-2-propoxide [Cu(dmap)<sub>2</sub>] and diethylzinc [Et<sub>2</sub>Zn] that  
37 was realized experimentally by Lee *et al.* [Angew. Chemie Int. Ed. **2009**, 48, 4536–4539]. We  
38 find that the Cu(dmap)<sub>2</sub> molecule adsorbs and dissociates through the scission of one or two Cu –  
39 O bonds into surface-bound dmap and Cu(dmap) fragments during the copper pulse. As Et<sub>2</sub>Zn  
40 adsorbs on the surface covered with Cu(dmap) and dmap fragments, butane formation and  
41 desorption was found to be facilitated by the surrounding ligands, which leads to one reaction  
42 mechanism, while the migration of ethyl groups to the surface leads to another reaction  
43  
44  
45  
46  
47  
48  
49  
50  
51  
52  
53  
54  
55  
56  
57  
58  
59  
60

1  
2  
3 mechanism. During both reaction mechanisms, ligand diffusion and reordering are generally  
4  
5 endothermic processes, which may result in residual ligands blocking the surface sites at the end  
6  
7 of the Et<sub>2</sub>Zn pulse, and in residual Zn being reduced and incorporated as an impurity. We also  
8  
9 find that the nearby ligands play a cooperative role in lowering the activation energy for  
10  
11 formation and desorption of by-products, which explains the advantage of using organometallic  
12  
13 precursors and reducing agents in Cu ALD. The ALD growth rate estimated for the mechanism  
14  
15 is consistent with the experimental value of 0.2 Å/cycle. The proposed reaction mechanisms  
16  
17 provide insight into ALD processes for copper and other transition metals.  
18  
19  
20  
21  
22  
23

## 24 **1. Introduction**

25  
26 The interest in depositing uniform and island-free ultrathin films of copper originates from its  
27  
28 application as the interconnect material in electronic devices. Copper has superior properties to  
29  
30 aluminium as an interconnect material, such as lower resistivity and higher current density for  
31  
32 electromigration, which are critical for improved device performance and reliability.<sup>1</sup> Deposition  
33  
34 techniques such as physical vapor deposition (PVD),<sup>2</sup> electrodeposition,<sup>3</sup> chemical vapor  
35  
36 deposition (CVD)<sup>4</sup> and atomic layer deposition (ALD)<sup>5-8</sup> have been applied with the aim of  
37  
38 obtaining a thin film of Cu. It is extremely difficult to deposit continuous thin films of Cu at 2  
39  
40 nm thickness and instead formation of Cu islands with size of 10-90 nm tends to be more  
41  
42 favourable.<sup>9</sup> Of these deposition approaches, ALD shows the most promise in surmounting the  
43  
44 island growth problem as well as meeting future demands of device scaling.<sup>10-12</sup>  
45  
46  
47  
48  
49

50 Many copper organometallic compounds are used with H<sub>2</sub> or H<sub>2</sub> plasma in copper ALD  
51  
52 experiments<sup>13-18</sup>. However, these processes lead to impurities and discontinuous films either  
53  
54 because of the higher temperature requirement or because of the strong reducing or oxidizing  
55  
56 nature of the co-reagents.<sup>8,19,20</sup> Significant progress was made by Lee *et al.* in developing low  
57  
58  
59  
60

1  
2  
3 temperature ALD of copper metal using the reaction of copper dimethylamino-2-propoxide  
4 [Cu(dmap)<sub>2</sub>] and diethylzinc [Et<sub>2</sub>Zn] at 100–120 °C.<sup>21</sup> Although subsequent work reported that  
5  
6 the parasitic CVD reaction of Et<sub>2</sub>Zn may lead to Zn incorporation into the copper thin film,<sup>20</sup> the  
7  
8 work by Lee *et al.* has important implications on the co-reagent strategy which was traditionally  
9  
10 limited to the use of molecular or plasma H<sub>2</sub>. The reaction of Cu(dmap)<sub>2</sub> and Et<sub>2</sub>Zn was  
11  
12 previously used to synthesize Cu/Zn alloy nanocolloids using thermolysis.<sup>22</sup> Vidjayacoumar *et*  
13  
14 *al.* investigated ALD reactions of eight different copper (II) complexes separately with AlMe<sub>3</sub>,  
15  
16 BEt<sub>3</sub> and Et<sub>2</sub>Zn in order to identify the most promising combination of the copper precursor and  
17  
18 co-reagent.<sup>20,23</sup> The reductive properties of various metallocenes along with different copper  
19  
20 precursors were investigated with density functional theory (DFT) and solution phase chemistry  
21  
22 to evaluate the use of metallocene compounds as reducing agents for Cu ALD.<sup>24</sup>  
23  
24  
25  
26  
27  
28

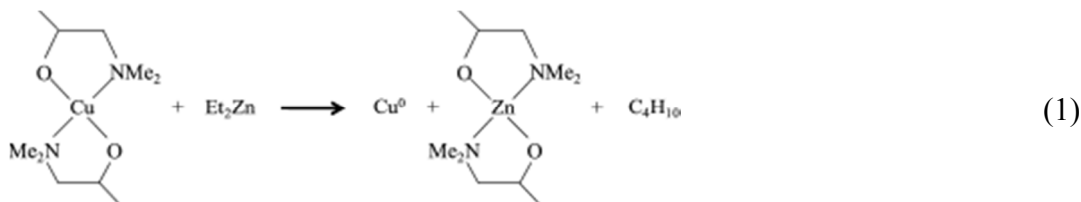
29 Cu(dmap)<sub>2</sub> has been a popular choice for other Cu ALD processes. For example, Knisley *et al.*  
30  
31 reported a low temperature three-step ALD process using Cu(dmap)<sub>2</sub>, formic acid (HCO<sub>2</sub>H) and  
32  
33 hydrazine (N<sub>2</sub>H<sub>4</sub>) at 120 °C and indicated that their method can avoid undesired elements in the  
34  
35 precursors and affords high purity low resistivity copper metal.<sup>6</sup> Kalutarage *et al.* compared two-  
36  
37 step and three-step processes using the ALD reaction of Cu(dmap)<sub>2</sub> with BH<sub>3</sub>(NHMe<sub>2</sub>) and  
38  
39 separately with BH<sub>3</sub>(NHMe<sub>2</sub>) and HCO<sub>2</sub>H.<sup>9</sup> They showed that the two-step process requires a Cu  
40  
41 seed layer, and affords a growth rate of about 0.13 Å/cycle within the 130–160 °C ALD window.  
42  
43 The three-step process does not need a Cu seed layer for growth, and affords a growth rate of  
44  
45 0.20 Å/cycle within the 135–165 °C ALD window. Guo *et al.* explored an ALD process for  
46  
47 depositing copper thin film on silicon wafers and glass slides at 50 °C using copper(I)-N,N'-  
48  
49 diisopropylacetamidinate precursor and H<sub>2</sub> plasma.<sup>25</sup> The focus in many of those experimental  
50  
51 works is on the deposition and characterization of copper thin films, with less elaboration of the  
52  
53  
54  
55  
56  
57  
58  
59  
60

1  
2  
3 self-terminating surface reactions that are important requirement for an ALD process.  
4  
5 Computational studies such as electronic structure calculations can be an efficient way to  
6  
7 investigate the surface reactions during ALD and provide useful information to develop better  
8  
9 processes.<sup>26</sup> For instance, developing a model for island formation will require knowledge of the  
10  
11 kinetics of the underlying deposition reactions.  
12  
13

14  
15 Although the ALD mechanisms of metal oxides are well understood,<sup>27–29</sup> very few  
16  
17 theoretical<sup>30–32</sup> and *in situ* experimental<sup>33,34</sup> works have been dedicated to understand the reaction  
18  
19 mechanisms of copper and related metals. Dey *et al.* used a gas phase model to study the  
20  
21 reactions of several common Cu precursors with Et<sub>2</sub>Zn.<sup>30</sup> Copper(I) carbene hydride complexes  
22  
23 which act both as reducing agent and precursor for Cu ALD were proposed by Dey *et al.* in a gas  
24  
25 phase density functional theory (DFT) study.<sup>35</sup> However, since ALD is based on self-  
26  
27 terminating surface reactions, it is necessary to understand the role of the surface. Dey *et al.* also  
28  
29 investigated the surface reactions of several copper precursors and diethylzinc to identify an  
30  
31 effective ALD process.<sup>36</sup> They found that dmap-type ligands are best for ALD of copper while  
32  
33 the reducing agent Et<sub>2</sub>Zn is not a good choice because it dissociates into ZnEt and Et fragments  
34  
35 on a bare copper surface, which may result in the Zn impurity observed in experimental work.  
36  
37 Hu *et al.* compared the adsorption of (<sup>n</sup>Bu<sub>3</sub>P)<sub>2</sub>Cu(acac) and Cu(acac)<sub>2</sub> precursors on Ta(110)  
38  
39 surface using DFT calculations and found that the (<sup>n</sup>Bu<sub>3</sub>P)<sub>2</sub>Cu(acac) precursor prefers to  
40  
41 dissociate in the gas phase while Cu(acac)<sub>2</sub> favours decomposition on the Ta surface.<sup>37</sup> Recently,  
42  
43 Hu *et al.* studied the surface chemistry of copper metal and copper oxide ALD from copper(II)  
44  
45 acetylacetonate [Cu(acac)<sub>2</sub>] and different co-reagents (e.g. H<sub>2</sub>, atomic H and H<sub>2</sub>O) using periodic  
46  
47 DFT and reactive molecular dynamics.<sup>38</sup> Ma *et al.* found that the ligands of Cu(acac)<sub>2</sub>  
48  
49 decompose when they adsorb onto bare Cu.<sup>39</sup>  
50  
51  
52  
53  
54  
55  
56  
57  
58  
59  
60

1  
2  
3 In a previous publication, we explained how ALD deposited copper oxide thin films can be  
4 reduced to metallic copper through oxygen vacancy formation and H<sub>2</sub> adsorption.<sup>40</sup> Previously,  
5 we also studied the adsorption of Cu(dmap)<sub>2</sub> on flat and rough copper surfaces using DFT with  
6 different treatments of van der Waals (vdW) interaction.<sup>41,42</sup> We found that the adsorption  
7 energies and geometries of the Cu(dmap)<sub>2</sub> adsorbed on the Cu surfaces depend substantially on  
8 the adsorption sites and treatment of vdW interactions. Based on this in-depth investigation of  
9 the precursor, we now proceed to study the full ALD reaction cycle using Cu(dmap)<sub>2</sub> and the  
10 Et<sub>2</sub>Zn co-reagent.  
11  
12  
13  
14  
15  
16  
17  
18  
19  
20  
21

22 In their original work, Lee *et al* proposed a transmetalation reaction of Cu(dmap)<sub>2</sub> and Et<sub>2</sub>Zn,  
23 which yields metallic copper and by-products Zn(dmap)<sub>2</sub> and butane as shown in Equation (1):  
24  
25  
26



Because the ALD mechanism of the reaction in Equation (1) is not clear, we compare the  
reaction mechanisms of Al<sub>2</sub>O<sub>3</sub> ALD and its analogy for Cu ALD, which are shown in Figure 1.  
Al<sub>2</sub>O<sub>3</sub> ALD is a well-known model system for explaining ALD in general.<sup>27,43,44</sup> The Al<sub>2</sub>O<sub>3</sub> ALD  
growth consists of alternating exposure of trimethylaluminum (TMA) and H<sub>2</sub>O (Figure 1a). Note  
that the partition of each pulse into two steps (a, b) is conceptual. Each step may be self-limiting  
– i.e. there are two ways to achieve self-limiting ALD. During the first pulse, TMA reacts with  
the hydroxyl groups on the substrate to deposit Al<sub>2</sub>O<sub>3</sub> and form CH<sub>4</sub> by-product (step 1a). Even  
when all hydroxyl groups have reacted, TMA continues to adsorb on the newly formed Al<sub>2</sub>O<sub>3</sub>  
surface until the surface is fully saturated with CH<sub>3</sub> groups (step 1b). Notice that s-Al(CH<sub>3</sub>)

represents any TMA fragments, *e.g.*  $\text{Al}(\text{CH}_3)_2$ . During the water pulse,  $\text{H}_2\text{O}$  reacts with the  $\text{Al}(\text{CH}_3)$  covered surface to form  $\text{Al}_2\text{O}_3$  (step 2a). Further adsorption of  $\text{H}_2\text{O}$  on the  $\text{Al}_2\text{O}_3$  surface results in the surface saturated with OH groups (step 2b), which completes a full reaction cycle.

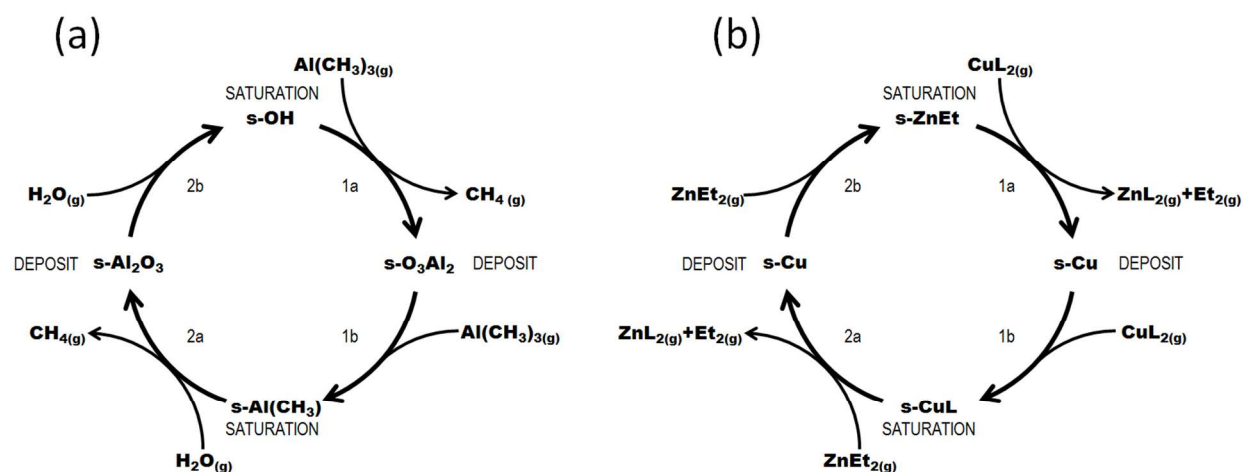


Figure 1. Schematic illustrations of (a) the known  $\text{Al}_2\text{O}_3$  ALD mechanism and (b) Cu ALD from Equation 1. Surface species are labelled with 's-' and 'L' represents the dmap ligand in (b).

In Figure 1a, the  $\text{Al}_2\text{O}_3$  ALD mechanism is represented with separate ligand elimination and ligand saturation steps in each cycle. Applying the same representation to the ALD of Cu, it is possible to propose a cyclic process for the reaction between  $\text{CuL}_2$  ( $\text{L}=\text{dmap}$ ) and  $\text{Et}_2\text{Zn}$ , as shown in Figure 1b. During the copper pulse, it is proposed in Eq. 1 that the  $\text{CuL}_2$  reacts with the  $\text{ZnEt}$  covered surface to form metallic copper and gives by-products of  $\text{ZnL}_2$  and butane (step 1a). The  $\text{CuL}_2$  decomposes on the surface to form  $\text{CuL}$  covered surfaces (step 1b). As  $\text{Et}_2\text{Zn}$  is admitted in step 2a, direct analogy with the oxide ALD would in fact give Zn impurity as the deposited product and  $\text{dmap-Et}$  as by-product. However, Eq. 1 instead proposes that Cu is deposited by transmetalation and the Zn is etched away as  $\text{ZnL}_2$ , as shown in Figure 1b. The success of transmetalation is based on the Cu compound decomposing into butane + Cu.



1  
2  
3 Therefore, in the Zn pulse, adsorption of  $\text{Et}_2\text{Zn}$  (step 2a) leads to the same reaction as step 1a. In  
4  
5 step 2b, the further adsorbed  $\text{Et}_2\text{Zn}$  decomposes on the bare Cu surface to form a ZnEt covered  
6  
7 surface, ready for the next cycle.  
8  
9

10 Having postulated this reaction cycle, it is interesting to ask whether each step is  
11  
12 thermodynamically favourable and kinetically viable, but also whether each step self-limits as  
13  
14 required for ALD, or whether competing reactions play an important role. We would also like to  
15  
16 estimate the ALD growth rate for this reaction cycle and compare it with experiment. The  
17  
18 amount of Cu deposited in each cycle will be limited by the saturating coverage of Et ligands  
19  
20 (prior to step 1a) and the saturating coverage of dmap ligands (at the end of step 1b). However,  
21  
22 if surface diffusion of Et or dmap ligands is slow, then a saturating coverage may not be  
23  
24 achieved and the process will instead be limited by the availability of adsorption sites for  
25  
26  $\text{Cu}(\text{dmap})_2$  during these steps.  
27  
28  
29  
30

31 In this work, we use the periodic DFT method to investigate the kinetics and reaction  
32  
33 mechanism of the Cu ALD proposed in Figure 1b. To this end, we calculate the activation  
34  
35 barriers ( $E_a$ ) and reaction energies ( $\Delta E$ ) of a series of surface reactions to study the reaction  
36  
37 pathways and energetics for a full cycle of the surface reaction of  $\text{Cu}(\text{dmap})_2$  and  $\text{Et}_2\text{Zn}$  in  
38  
39 Equation (1). We will start the process with step 1b, namely the adsorption and decomposition of  
40  
41  $\text{Cu}(\text{dmap})_2$  precursor on bare Cu surfaces. We show that the  $\text{Cu}(\text{dmap})_2$  dissociates, through the  
42  
43 scission of Cu – O bonds and produces dmap and  $\text{Cu}(\text{dmap})$  fragments that saturate the surface  
44  
45 in the first pulse. Butane formation with the assistance of ligands and the diffusion of ethyl  
46  
47 groups on the surface can lead to different reaction mechanisms during the steps when ligands  
48  
49 mix on the surface (step 2a of the  $\text{Et}_2\text{Zn}$  pulse and step 1a of the  $\text{CuL}_2$  pulse), because of the  
50  
51 different surface coverage of dmap ligands. We demonstrate that the activation energies for the  
52  
53  
54  
55  
56  
57  
58  
59  
60

1  
2  
3 formation and desorption of  $\text{Et}_2\text{Zn}$  and  $\text{Zn}(\text{dmap})_2$  by-products are lowered by nearby ligands,  
4 which explains the advantage of using organometallic precursors and reducing agents in Cu  
5 ALD. The proposed ALD mechanisms provide insight into how to achieve the ALD of copper  
6 and other transition metals.  
7  
8  
9  
10  
11

## 12 13 14 15 **2. Computational Method** 16

17  
18 All calculations were performed using the Vienna Ab Initio Simulation Package (VASP  
19 5.3).<sup>45,46</sup> Projector augmented wave (PAW)<sup>47</sup> potentials were used to represent the effective core  
20 electrons and nuclei. Electronic optimization was performed self-consistently using the plane  
21 wave basis set with a cutoff energy of 450 eV for the valence electrons. The  
22 Perdew–Burke–Ernzerhof (PBE)<sup>48</sup> functional was used to describe exchange and correlation  
23 effects. The impact of vdW forces on activation barriers and reaction energies is also assessed for  
24 some cases using vdW-optB88<sup>49,50</sup> and the choice of vdW-optB88 is justified in Ref<sup>41</sup>. The  
25 effect of spin polarization was found to be negligible for tests on the activation and reaction  
26 energies and thus non-spin-polarized calculations were performed. It was also found to be  
27 adequate to use only the  $\Gamma$  point to sample the Brillouin zone for all the calculations because of  
28 the large cell sizes. The adsorption of  $\text{Cu}(\text{dmap})_2$  on the Cu(111) surface with the four layered  
29 (6.289 Å thick) slabs separated by 18 Å of vacuum was tested on three different supercells:  $p(4 \times$   
30 4),  $p(5 \times 5)$  and  $p(6 \times 6)$ . It is found that the  $\text{Cu}(\text{dmap})_2$  does not adsorb on  $p(4 \times 4)$  - Cu(111)  
31 surface. Although  $\text{Cu}(\text{dmap})_2$  chemisorbs on the bridge site on the Cu(111) surface with  $(5 \times 5)$   
32 expansion, the  $p(6 \times 6)$  supercell was chosen for this study so as to have space for  $\text{Et}_2\text{Zn}$  to  
33 adsorb as well. The simulation of one  $\text{Cu}(\text{dmap})_2$  and/or  $\text{Et}_2\text{Zn}$  within this supercell corresponds  
34 to a coverage of one molecule per surface area of  $2.0 \text{ nm}^2$  (cell volume =  $4.99 \text{ nm}^3$ ), following  
35  
36  
37  
38  
39  
40  
41  
42  
43  
44  
45  
46  
47  
48  
49  
50  
51  
52  
53  
54  
55  
56  
57  
58  
59  
60

our previous study in Ref <sup>41</sup>. A free area of about 2.0 nm<sup>2</sup> of bare Cu is thus required for molecular chemisorption of Cu(dmap)<sub>2</sub>. The electronic energy convergence criterion is 10<sup>-4</sup> eV, and all atoms in the slab were allowed to relax. The systems were considered to be fully optimized when the forces on each ion were smaller than 0.02 eV/Å.

The minimum energy pathways (MEP) were investigated using the climbing image nudged elastic band method (CI-NEB) to determine the transition state (TS) structure.<sup>51,52</sup> For both reactant and product of a certain reaction, we performed geometry optimization to identify the minimum energy configurations, which were then used to generate eight initial images along the MEP using linear interpolation. These atomic structures were relaxed subject to the CI-NEB constraints using the quasi-Newton scheme as the CI-NEB method requires a force-based optimizer.<sup>51,52</sup>

### 3. Results

This Cu ALD process consists of alternate pulses of precursor Cu(dmap)<sub>2</sub> and co-reagent Et<sub>2</sub>Zn, separated by purges so that the two reagents are never simultaneously present in the gas-phase. Their mutual reaction thus takes place via adsorbates. Since Cu(dmap)<sub>2</sub> and Et<sub>2</sub>Zn are introduced to the chamber in a sequential manner during the experiment, the full reaction cycle is divided into two sections. In section 3.1 we look at adsorption and decomposition (steps 1a and 1b) of Cu(dmap)<sub>2</sub> on bare Cu segments of the surface. In section 3.2 we investigate adsorption and decomposition of Et<sub>2</sub>Zn (steps 2a and 2b), along with the series of surface reactions taking place between mixed fragments of Cu(dmap)<sub>2</sub> and Et<sub>2</sub>Zn, followed by by-product formation and desorption (steps 1a and 2a). Step 1a thus regenerates a bare Cu(111) surface, ready for the repetition of step 1b. We therefore calculate the activation ( $E_a$ ) and reaction energies ( $\Delta E$ ) of a series of surface reactions of the Cu(dmap)<sub>2</sub> and Et<sub>2</sub>Zn on bare Cu(111) and identify reaction

1  
2  
3 pathways that have low enough activation energies to be viable at the experimental ALD  
4  
5 temperature (393 K) in Ref <sup>21</sup>. Based on these calculations, we combine the reaction routes and  
6  
7 propose the full ALD reaction cycle.  
8  
9

10 The steps in this cyclic process are labelled with capital letters from ‘A’ to ‘G’. In the  
11  
12 following sections, we separately present our results on each of these steps and discuss these  
13  
14 reactions in order to understand the overall reaction mechanism of Cu ALD. Table 1 lists the  
15  
16 calculated activation barrier ( $E_a$ ) and the reaction energy ( $\Delta E$ ) for the selected reactions of  
17  
18 Cu(dmap)<sub>2</sub> and Et<sub>2</sub>Zn on the Cu(111) surface. Table 1S in Supporting Information displays the  
19  
20 calculated activation barriers  $E_a > 1$  eV (and associated reaction energies) that are too high for  
21  
22 the surface reactions to occur in the ALD experiment.  
23  
24  
25  
26  
27  
28  
29

30 Table 1. The calculated activation barriers ( $E_a$ ) and reaction energies ( $\Delta E$ ) for possible reactions  
31  
32 for depositing Cu from Cu(dmap)<sub>2</sub> and Et<sub>2</sub>Zn through ALD. The data are plotted in Figure 2 and  
33  
34 Figure 4. Capital letters ‘A’ to ‘G’ represent the following steps leading to atomic structures  
35  
36 numbered A1, A2 etc: A is adsorption of Cu(dmap)<sub>2</sub> (Figure 3), B is decomposition of  
37  
38 Cu(dmap)<sub>2</sub> (Figure 3), C is adsorption of Et<sub>2</sub>Zn on the dmap-covered surface (Figure 5), D is the  
39  
40 ethyl group migration (Figure 7), E is ligand diffusion (Figure 8), F is ligand re-ordering (Figure  
41  
42 9), G and H are Zn(dmap)<sub>2</sub> or butane formation (Figure 10 and Figure 10). The reactions with  $E_a$   
43  
44 less than 1.0 eV are shown here and in the figures; those with  $E_a > 1$  eV are in Table 1S  
45  
46 (supporting information).  
47  
48  
49  
50  
51

reactions	$E_a$ (eV)	$\Delta E$ (eV)	explanation
Section 3.1			
1. A1		-0.39	Physisorption of Cu(dmap) <sub>2</sub> from gas phase

2. A1→A2	0.17	-1.01	Physisorption to chemisorption transition
3. A2→B1	0.44	-0.11	One Cu–O bond scission Cu(dmap) + dmap
4. A2→B2	0.58	-0.01	Double Cu–O bond scission dmap +Cu +dmap
Section 3.2			
5. B1→C1		-0.03	Et <sub>2</sub> Zn adsorption between Cu(dmap) + dmap
6. B2→C2		0.01	Et <sub>2</sub> Zn adsorption between dmap+ Cu + dmap
7. C1→D1	0.78	-2.03	Butane formation and desorption
8. C1→D2	0.55	-0.65	ZnEt, CuEt, Cu(dmap), dmap formation
9. C2→D2	0.57	-0.69	ZnEt, CuEt, Cu(dmap), dmap formation
10. C1→D3	0.61	0.31	Two ethyl groups attached to the surface
11. D1→E1	0.34	-0.33	dmap ligand diffusion
12. D1→E2	0.68	0.28	dmap ligand diffusion
13. D2→E3	0.85	-0.68	Butane formation
14. D3→E4	0.33	0.20	dmap ligands diffusion
15. E1→F1	0.44	0.37	dmap ligands diffusion
16. E2→F2	0.62	0.28	dmap ligands diffusion
17. E3→F3	0.71	0.35	dmap ligands diffusion
18. E4→F4	0.56	0.30	Zn(dmap) <sub>2</sub> formation
19. F1→G1	0.78	0.43	dmap ligands re-ordering
20. F2→G1	0.15	0.05	dmap ligands re-ordering
21. F3→G1	0.32	-0.83	dmap ligands re-ordering
22. F4→G2	0.49	-0.38	Ethyl groups re-ordering
23. G1→H1	0.79	0.72	Zn(dmap) <sub>2</sub> desorption
24. G2→H2	0.73	-1.49	Butane desorption

Adsorption energies of Et<sub>2</sub>Zn (reactions 5 and 6) on decomposed Cu(dmap)<sub>2</sub> is calculated relative to the configuration B1 with surface fragments of Cu(dmap) + dmap.

### 3.1. Adsorption and decomposition of Cu(dmap)<sub>2</sub> on Cu(111) surface

In the previous work, we studied the adsorption of Cu(dmap)<sub>2</sub> on a number of adsorption sites on flat and rough Cu surfaces using different levels of treatment of vdW interactions.<sup>41</sup> We found that pure PBE predicts that physisorbed and chemisorbed structures exist on the flat Cu(111) surface depending on the adsorption sites. We also found from the Bader charge analysis that the Cu atom in the molecule gains 0.2–0.4 electrons from the surface on chemisorption, which indicates that the adsorbate Cu atom is partially reduced when molecularly adsorbed. Now we discuss the possible reaction pathways of the adsorption of Cu(dmap)<sub>2</sub> onto segments of bare Cu(111) (configuration A) and its decomposition (configuration B) before reaction with Et<sub>2</sub>Zn adsorbates. The energetics are illustrated in Figure 2.

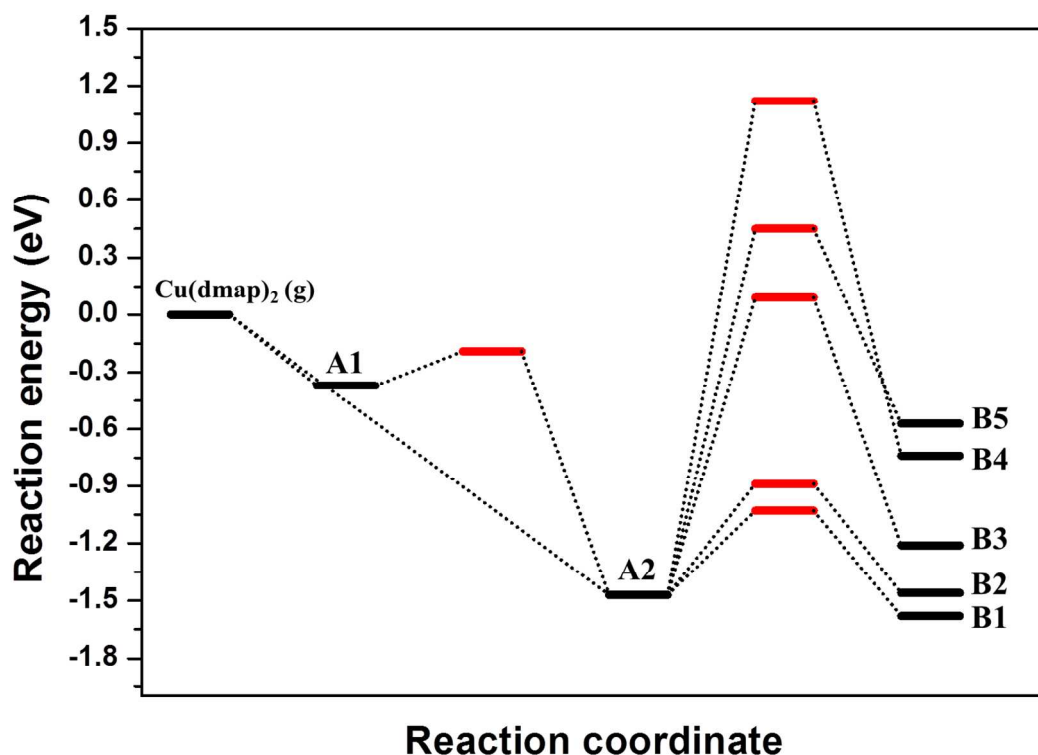


Figure 2. First half of the reaction cycle of Cu ALD for the Cu(dmap)<sub>2</sub> pulse. Reactant/product states are in black and activation energies are in red. Atomic structures for adsorption (A1, A2)

1  
2  
3 and decomposition (B1 and B2) are in Figure 3. The structures of B3, B4 and B5 are provided in  
4  
5  
6 Figure 1S.

7  
8  
9 **A: Adsorption of Cu(dmap)<sub>2</sub>.** The physisorbed (A1) and chemisorbed (A2) structures are  
10  
11 shown in Figure 3. The physisorbed Cu(dmap)<sub>2</sub> molecule is stable and not spontaneously  
12  
13 reactive to Et<sub>2</sub>Zn in our calculations. Therefore the physisorbed Cu(dmap)<sub>2</sub> molecules (A1)  
14  
15 should transform into chemisorbed states (A2) if ALD is to take place. This involves the loosing  
16  
17 of Cu – N coordination and the formation of metallic bonds from adsorbate Cu to surface Cu as  
18  
19 described in detail in Ref <sup>41</sup>. Figure 2 shows that the transformation needs a small activation  
20  
21 energy of 0.17 eV, which can be overcome at a typical ALD temperature, e.g. 100 °C.  
22  
23  
24  
25  
26  
27  
28  
29  
30  
31  
32  
33  
34  
35  
36  
37  
38  
39  
40  
41  
42  
43  
44  
45  
46  
47  
48  
49  
50  
51  
52  
53  
54  
55  
56  
57  
58  
59  
60

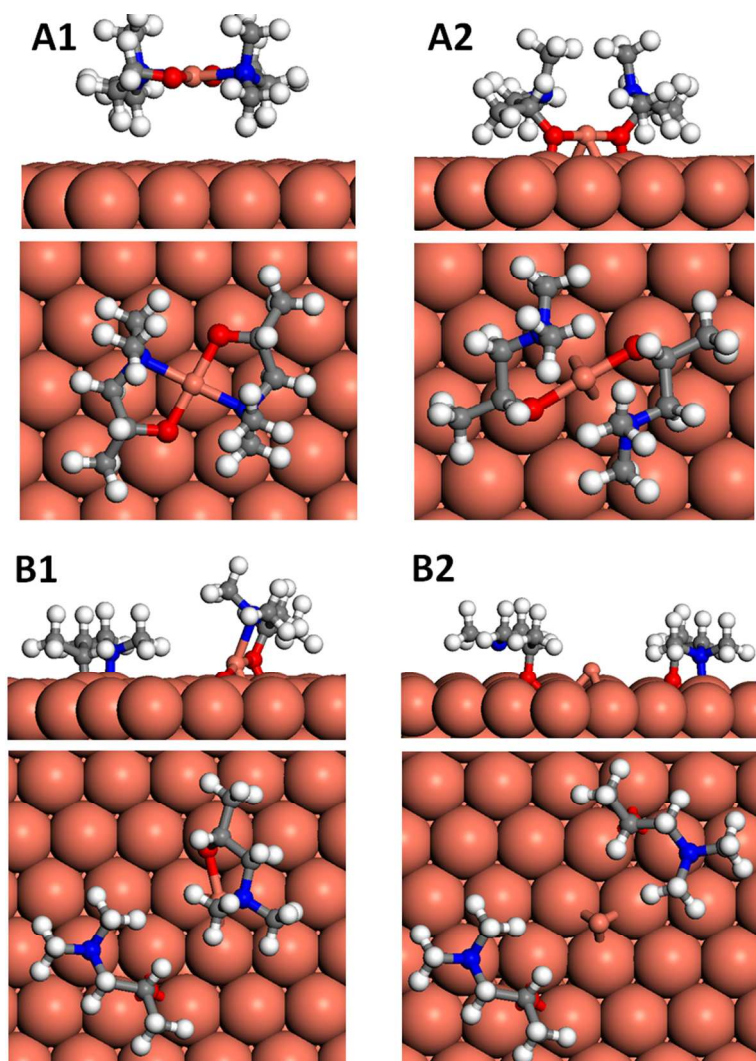


Figure 3. Adsorption (step A) and decomposition (step B) of  $\text{Cu}(\text{dmap})_2$  on one  $(6 \times 6)$  cell of the  $\text{Cu}(111)$  surface. A1 represents physisorption and A2 represents chemisorption. The fragments of decomposed  $\text{Cu}(\text{dmap})_2$  are  $\text{Cu}(\text{dmap}) + \text{dmap}$  (B1) and  $\text{dmap} + \text{Cu} + \text{dmap}$  (B2). The colour code used throughout the paper and Supporting Information is as follows: salmon pink = copper, red = oxygen, blue = nitrogen, grey = carbon and white = hydrogen.

**B: Decomposition of  $\text{Cu}(\text{dmap})_2$ .** The surface should be saturated with the chemisorbed  $\text{Cu}(\text{dmap})_2$  molecules or fragments after the  $\text{Cu}(\text{dmap})_2$  pulse in the ALD experiment. We found that  $\text{Et}_2\text{Zn}$  will not react with the chemisorbed  $\text{Cu}(\text{dmap})_2$  molecules on  $\text{Cu}(111)$ . This is because



1  
2  
3 the Cu centre of the molecule is still not accessible, although the  $\text{Cu}(\text{dmap})_2$  molecule is partially  
4 decomposed upon chemisorption. Thus, it is legitimate to assume that the chemisorbed  
5  $\text{Cu}(\text{dmap})_2$  undergoes further decomposition. We considered several possibilities for bond  
6 scissions in the  $\text{Cu}(\text{dmap})_2$  molecule: one Cu–O bond (B1), both Cu–O bonds (B2), O–C bond  
7 (B3), C–C bond (B4) and C–N bond (B5). We calculated the activation barriers for breaking one  
8 (A2→B1) and two (A2→B2) Cu–O bonds to be 0.44 eV and 0.58 eV, respectively, indicating  
9 that the reactions are both slow but viable at ALD temperatures. It was previously found that the  
10 dissociation of one acac ligand from  $\text{Cu}(\text{acac})_2$  on the Cu(110) surface requires an activation  
11 energy of 0.59 eV from PBE,<sup>38</sup> which is comparable to our finding for the dissociation of dmap  
12 ligand from  $\text{Cu}(\text{dmap})_2$  on Cu(111).

13  
14  
15  
16  
17  
18  
19  
20  
21  
22  
23  
24  
25  
26  
27 The optimized structures for the resulting configurations B1 and B2 are shown in Figure 3. In  
28 configuration B1, the surface is covered with the dmap and  $\text{Cu}(\text{dmap})$  fragments of the molecule.  
29 The distance between the O atom in dmap and the Cu atom in  $\text{Cu}(\text{dmap})$  is 4.45 Å, indicating  
30 that the Cu–O bond has broken. The O atom in the dmap is located in the hollow site of the  
31 Cu(111) surface and bonds with three surface Cu atoms. The Cu–N bond is re-formed (2.10 Å)  
32 again in the  $\text{Cu}(\text{dmap})$  fragment because of a reduction of strain in the molecule upon the  
33 dissociation of the other dmap ligand.

34  
35  
36  
37  
38  
39  
40  
41  
42  
43  
44 In configuration B2, the distances of the O atoms in the dmap fragments from the adsorbate Cu  
45 atom are 3.95 Å and 3.99 Å, again indicating complete dissociation. Both the O atoms in the  
46 dmap fragments are bonding to Cu atoms of a hollow site. A bond between N and Cu surface  
47 atom is formed (2.31 Å) in one of the dmap ligands as is evident from Figure 3 where the Cu  
48 surface atom under the N atom is pulled up significantly. By comparing configurations B1 and  
49 B2 in Figure 3, we can see that the B1 configuration has a more dense coverage of dmap ligands  
50  
51  
52  
53  
54  
55  
56  
57  
58  
59  
60

1  
2  
3 in the immediate locality of the Cu atom than the B2 configuration. Later we will show that this  
4  
5 difference in the density of the ligands leads to two different reaction pathways. The reverse  
6  
7 reaction to form the  $\text{Cu}(\text{dmap})_2$  molecule from these decomposed fragments is extremely  
8  
9 unlikely because the forward reaction energies ( $\Delta E$ ) of  $\text{A1} \rightarrow \text{B1}$  and  $\text{A1} \rightarrow \text{B2}$  reactions are  
10  
11 around -1.5 eV.  
12  
13

14  
15 We now consider decomposition of a dmap ligand from chemisorbed  $\text{Cu}(\text{dmap})_2$  (A2). The  
16  
17 calculated activation energies are 1.56 eV for the scission of the O–C bond ( $\text{A2} \rightarrow \text{B3}$ ), 1.92 eV  
18  
19 for the scission of C–C bond ( $\text{A2} \rightarrow \text{B4}$ ) and 2.59 eV for the scission of C–N bond ( $\text{A2} \rightarrow \text{B5}$ ) (see  
20  
21 Table S1 in Supporting information). The optimized structures of B3, B4 and B5 are displayed in  
22  
23 Figure S1 in Supporting Information. Based on these  $E_a$ , the breaking of the O–C, C–C and C–N  
24  
25 bonds are not accessible at a typical ALD reaction temperature of 100 °C, as in the work of Lee  
26  
27 *et al.*<sup>21</sup> This indicates that the  $\text{Cu}(\text{dmap})_2$  molecules fragment instead through the breaking of one  
28  
29 or two Cu–O bonds (B1 and B2) in ALD experiments. This shows that dmap ligands are  
30  
31 ‘innocent’ and participate in the reaction as a single unit. Therefore in this work, decomposition  
32  
33 of  $\text{Cu}(\text{dmap})_2$  refers to the dissociation of one or two Cu–O bonds in the  $\text{Cu}(\text{dmap})_2$  and not to  
34  
35 break-up of dmap itself. At the end of the  $\text{Cu}(\text{dmap})_2$  pulse, we expect that the Cu(111) surface is  
36  
37 saturated with the dmap and  $\text{Cu}(\text{dmap})$  fragments of the precursor and that the further adsorption  
38  
39 of  $\text{Cu}(\text{dmap})_2$  onto this surface is not possible due to Pauli repulsion. Therefore, as the  $\text{Et}_2\text{Zn}$   
40  
41 pulse starts, the  $\text{Et}_2\text{Zn}$  molecules may react simultaneously with the surface covered with  
42  
43 partially and fully dissociated  $\text{Cu}(\text{dmap})_2$ , namely  $\text{Cu}(\text{dmap}) + \text{dmap}$  (B1) and  $\text{dmap} + \text{Cu} +$   
44  
45  $\text{dmap}$  (B2). B1 and B2 represent surfaces with different surface coverage of  $\text{Cu}(\text{dmap})_2$   
46  
47 precursors in the locality of Cu.  
48  
49  
50  
51  
52  
53  
54  
55

### 56 **3.2. $\text{Et}_2\text{Zn}$ adsorption, butane formation and $\text{Zn}(\text{dmap})_2$ formation**

57  
58  
59  
60

Step 2a of the Cu ALD transmetalation process is proposed to be the reaction of  $\text{Et}_2\text{Zn}$  on the surface covered with fragments of  $\text{Cu}(\text{dmap})_2$  so as to deposit atomic Cu and formation of by-products butane and  $\text{Zn}(\text{dmap})_2$  (Equation 1). Step 1a consists of similar reactions of mixed ligands on a surface to reduce Cu and form by-products. We also investigate the formation of undesired by-products, which may result from parasitic reactions. Figure 4 shows the reaction energy pathways and values of activation and reaction energies are listed in Table 1, which we discuss in detail.

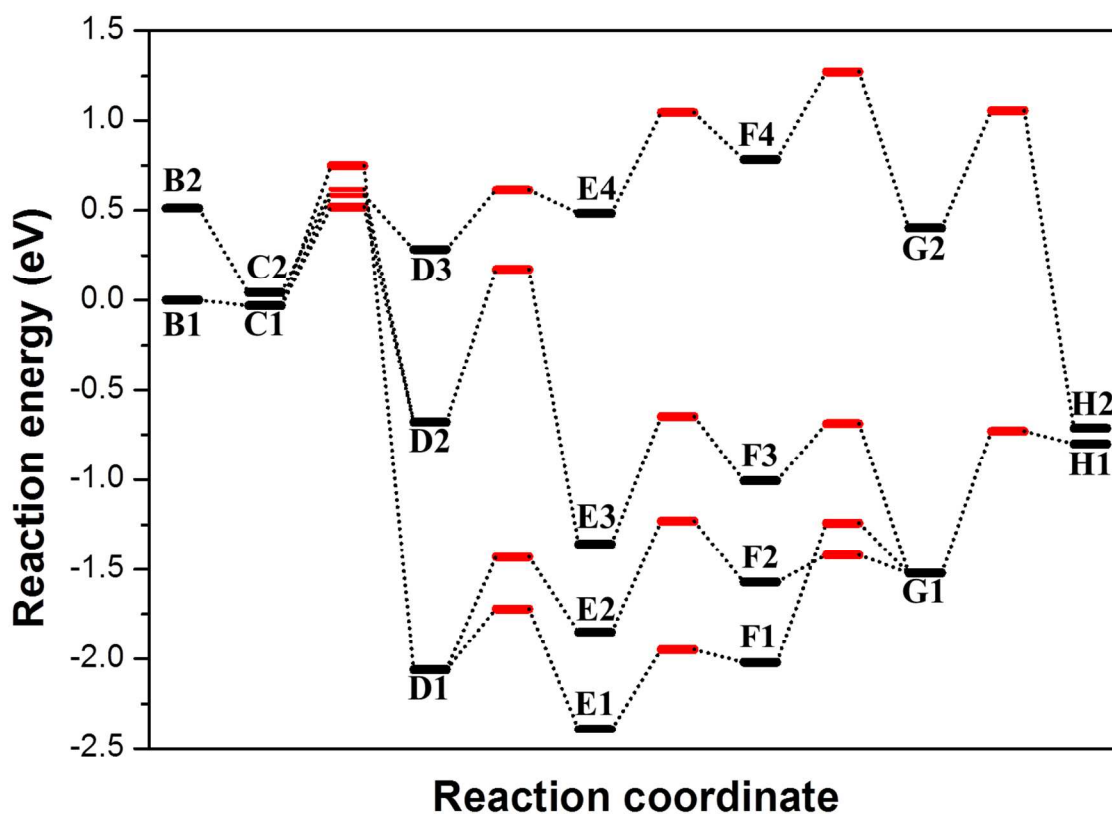


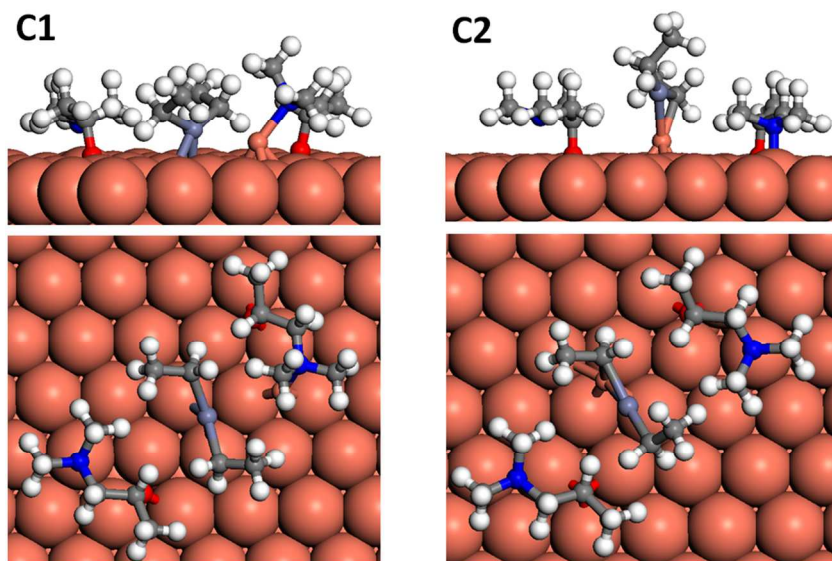
Figure 4. Reaction energy diagram for the second half reaction cycle of the Cu ALD process when  $\text{Et}_2\text{Zn}$  is admitted. Reactant/product states are in black and activation energies are in red. Forward activation energies greater than 1 eV are not included in the graph. The configurations labelled with a capital letter and number are shown in the following figures.

1  
2  
3 **C: Adsorption of Et<sub>2</sub>Zn on the dmap-covered surface (step 2a).** Figure 5 shows the  
4 optimized structures of Et<sub>2</sub>Zn adsorption on the configurations B1 and B2, which are labelled C1  
5 and C2, respectively. The adsorption energies are calculated to be -0.03 eV and +0.01 eV,  
6 respectively. These small adsorption energies are apparently the result of distortions of both  
7 dmap ligands and of the Et<sub>2</sub>Zn molecule on the surface. In the C1 configuration, the Et<sub>2</sub>Zn  
8 molecule is adsorbed between the Cu(dmap) and dmap fragments. The Zn atom in the Et<sub>2</sub>Zn  
9 molecule is situated on a bridge site of Cu(111). The ethyl groups are bent upward and the ∠C-  
10 Zn-C angle is 134.5°. The distance between Zn and the adsorbate Cu atom is 3.11 Å. The Zn – O  
11 distances are 4.01 Å and 4.35 Å. Notice that the ethyl groups in configuration C1 have no  
12 chemical bond with the surface. In configuration C2, the Et<sub>2</sub>Zn molecule is attached on top of the  
13 adsorbate Cu atom. The adsorbate Cu atom forms bonds with the Zn atom (Zn–Cu bond length is  
14 2.43 Å) and with the C atom (C –Cu bond length is 2.12 Å) in one of the ethyl groups to form a  
15 3-membered ring. This results in substantial stabilization relative to B2. The difference in the  
16 adsorption geometry between C1 and C2 results from the lower local coverage of the dmap  
17 ligands on the C2 surface. As will be shown in the next section, this has a substantial effect on  
18 subsequent reaction kinetics. However, overall, the C1 and C2 structures are very close in  
19 energy.

20  
21  
22  
23  
24  
25  
26  
27  
28  
29  
30  
31  
32  
33  
34  
35  
36  
37  
38  
39  
40  
41  
42  
43  
44 In the C1 and C2 structures, Et<sub>2</sub>Zn is found to adsorb on Cu atoms close to Cu(dmap)<sub>2</sub>  
45 fragments. This is because we assume that before step 2a the surface is saturated with the  
46 Cu(dmap)<sub>2</sub> precursor after the first pulse. (See reaction E→F below for the kinetics of dmap  
47 diffusion). However, during an ALD experiment dmap should desorb as Zn(dmap)<sub>2</sub> and the  
48 coverage of dmap will drop, and therefore the Et<sub>2</sub>Zn molecules of step 2b may adsorb on a bare  
49 segment of the surface. Thus, we also investigate the adsorption of Et<sub>2</sub>Zn on the fully bare  
50  
51  
52  
53  
54  
55  
56  
57  
58  
59  
60

1  
2  
3 Cu(111) surface. The  $\text{Et}_2\text{Zn}$  molecules decompose into Et and ZnEt fragments spontaneously  
4 upon adsorption onto Cu(111) without the presence of  $\text{Cu}(\text{dmap})_2$  fragments (see the adsorption  
5 structure in Figure S2, Supporting information) and the adsorption energy is -0.83 eV. This mode  
6 of decomposition of  $\text{Et}_2\text{Zn}$  into Et and ZnEt fragments structure was also found in previous *ab*  
7 *initio* molecular dynamics study on a model of bare Cu(111).<sup>36</sup>

8  
9  
10  
11  
12  
13  
14  
15 This indicates that the presence of  $\text{Cu}(\text{dmap})_2$  fragments (B1 and B2) prevents the full  
16 decomposition of  $\text{Et}_2\text{Zn}$  and permits that the Et groups to stay attached to the Zn atom, as shown  
17 in the C1 and C2 structures. The  $\text{Cu}(\text{dmap})_2$  fragments are affected by the adsorption of the  
18  $\text{Et}_2\text{Zn}$  molecule as the  $\text{CH}_3$  parts of the dmap ligands shift slightly upward.



45  
46 Figure 5. Step C: Adsorption of  $\text{Et}_2\text{Zn}$  on the surface with fragments of  $\text{Cu}(\text{dmap})_2$  from B1 and  
47 B2, respectively.  
48  
49  
50  
51  
52  
53  
54  
55  
56  
57  
58  
59  
60

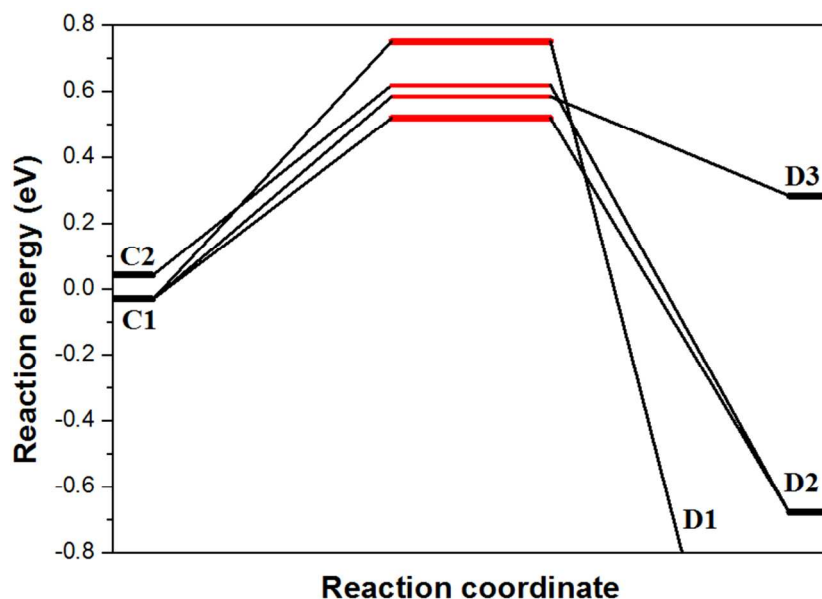


Figure 6. Reaction energy diagram from step ‘C’ to step ‘D’. This is the magnification of the process from ‘C’ to ‘D’ in Figure 4.

**D: The ethyl group migration (step 1a & 2a).** As the Zn atom is attached to ethyl groups in configurations C1 and C2, the ethyl groups must migrate away from the Zn atom in order to give the dmap ligand access to Zn and allow the ethyl groups to form butane, one of the by-products of Equation (1). We consider several possibilities for ethyl group migration: (1) direct butane formation from Zn and desorption (C1→D1); (2) one ethyl migration to adsorbate Cu to form CuEt and ZnEt fragments (C1→D2 and C2→D2) and (3) migration of both ethyl groups to surface Cu (C1→D3). The reaction energy diagram for this part is magnified from Figure 4 and shown in Figure 6 and the final configurations D1, D2 and D3 of ethyl group migrations are shown in Figure 7.

The direct formation of butane (C1→D1) is highly exothermic ( $\Delta E = -2.03$  eV, Table 1), and needs activation energy of 0.78 eV. (The reaction energy profile of this step is plotted in Figure S2 in Supporting Information). Electrons are transferred from desorbing ethyl groups to the

1  
2  
3 surface Zn atom. The distance between butane molecule and the surface in the D1 structure is 5.6  
4  
5 Å, indicating that the butane molecule has no interaction with the surface and can be purged  
6  
7 away during ALD experiment. The deposited Zn atom forms a bond with the Cu adatom with the  
8  
9 bond length of 2.6 Å. This direct formation of butane is a less likely scenario from configuration  
10  
11 C2, as evidenced by the calculated activation barrier of 1.25 eV (C2→D1, Table S1, Supporting  
12  
13 Information). This is because an extra C – Cu bond was formed when the Et<sub>2</sub>Zn adsorbed on the  
14  
15 Cu adatom in configuration C2. This is an important result because it shows the effect of surface  
16  
17 coverage (C2 vs C1) on the kinetics of formation of butane. As noted in the previous results, at  
18  
19 very low coverage, *i.e.* on segments of bare Cu, Et<sub>2</sub>Zn dissociates spontaneously into ZnEt +  
20  
21 CuEt, resulting in an even higher barrier to Et formation.  
22  
23  
24  
25  
26

27 In the second case, formation of CuEt and ZnEt fragments attached to the surface  
28  
29 (configuration D2) was achieved from both C1 and C2, with activation energies of 0.55 eV and  
30  
31 0.57 eV, and reaction energies of  $\Delta E = -0.7$  eV. In the C1→D2 reaction, one Et group from the  
32  
33 adsorbed Et<sub>2</sub>Zn migrates to the Cu adatom in Cu(dmap), which in turn causes the Cu-N bond to  
34  
35 break, displacing the dmap ligand to bind with surface Cu. The D2 surface is thus covered with  
36  
37 four fragments: two dmap ligands, ZnEt and CuEt groups. The ZnEt part of Et<sub>2</sub>Zn molecule  
38  
39 migrates to the surface by scission of C-Zn and Cu-Zn bonds.  
40  
41  
42  
43

44 The configuration D3, where the two ethyl groups have migrated to the Cu(111) surface, was  
45  
46 reached from configuration C1 with an activation energy of 0.61 eV and reaction energy of  
47  
48 +0.31 eV. Thermodynamics thus favours the reverse reaction from D3 to C1, or indeed to D2.  
49  
50 We found that achieving D3 from C2 is kinetically impossible, requiring an activation energy of  
51  
52 1.78 eV (Table S1 of Supporting Information), probably because this would re-expose the  
53  
54 adsorbate Cu atom.  
55  
56  
57  
58  
59  
60

1  
2  
3 Now we consider butane formation when no  $\text{Cu}(\text{dmap})_2$  fragments are around the adsorbed  
4  $\text{Et}_2\text{Zn}$  so as to quantify the role of  $\text{Cu}(\text{dmap})_2$  fragments on the energetics of butane formation.  
5  
6 Figure S2(b) displays the reaction energy profile of butane formation on the bare  $\text{Cu}(111)$   
7 surface. Without the  $\text{dmap}$  ligands, butane formation needs higher activation energy and is less  
8 exothermic ( $E_a = 0.99$  eV and  $\Delta E = -1.14$  eV) compared to the butane formation (C1→D1) from  
9 the  $\text{Et}_2\text{Zn}$  adsorbed in the neighbourhood of  $\text{Cu}(\text{dmap})_2$  fragments (see also Table S1, Supporting  
10 Information). We can explain this by noting that the adsorbed  $\text{Et}_2\text{Zn}$  decomposes into Et and  
11 ZnEt fragments when adsorbed on the bare surface, so that the formation of butane apparently  
12 becomes more difficult because breaking the C – Cu surface bond needs extra energy. The  
13 distance between the butane molecule and the surface with the presence of  $\text{Cu}(\text{dmap})_2$  fragments  
14 is longer by 1.4 Å compared to that on the bare  $\text{Cu}(111)$  surface. Thus, butane formation requires  
15 lower  $E_a$  when the  $\text{Cu}(\text{dmap})_2$  fragments are nearby. This indicates that the  $\text{dmap}$  ligands play a  
16 cooperative role<sup>53</sup> for the formation of butane.  
17  
18  
19  
20  
21  
22  
23  
24  
25  
26  
27  
28  
29  
30  
31  
32  
33  
34  
35  
36  
37  
38  
39  
40  
41  
42  
43  
44  
45  
46  
47  
48  
49  
50  
51  
52  
53  
54  
55  
56  
57  
58  
59  
60



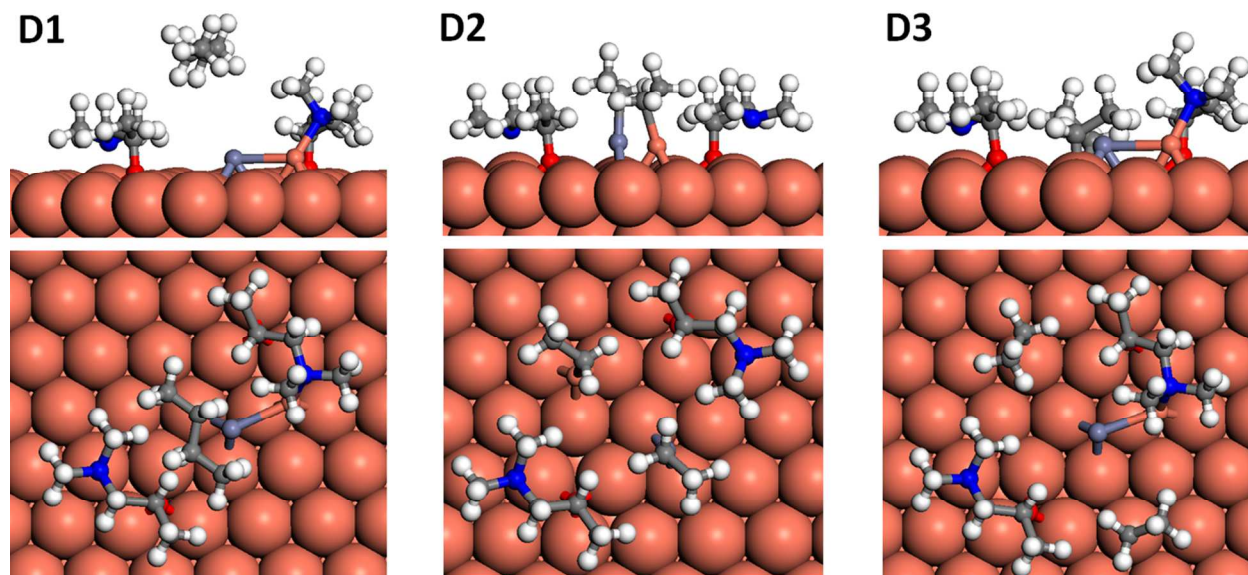


Figure 7. Step D: reaction of  $\text{Et}_2\text{Zn}$  obtained from configuration C1 and C2. Three possibilities are considered: D1 is butane formation; D2 is  $\text{ZnEt} + \text{CuEt}$  fragment formation and D3 has fragments of two ethyl groups on the  $\text{Cu}(111)$  surface.

A visual inspection of configurations D2 and D3 (Figure 7) shows that there is space in the ( $6 \times 6$ ) simulation cell for two adsorbed ethyl groups and two dmap ligands. It should therefore be possible to accommodate at least four ethyl groups in such a cell when dmap has been eliminated, even if diffusion of Et groups is slow. We use this result later to estimate the ALD growth rate.

**E: ligand diffusion.** Once the Zn atom becomes accessible for dmap ligands, dmap ligands may diffuse on the surface to form a  $\text{Zn}(\text{dmap})_2$  molecule, which is the other by-product in equation (1). Figure 8 shows the configurations of relevant reaction products obtained from D1, D2 and D3 configurations. The configurations E1 and E2 are obtained from D1 by moving dmap ligands after removing the butane molecule. In configuration E1, a dmap ligand moves toward the Zn atom (D1 $\rightarrow$ E1), which involves an activation energy of 0.34 eV and reaction energy of  $\Delta E = -0.33$  eV. This low barrier shows that dmap ligands can diffuse on the bare  $\text{Cu}(111)$  surface

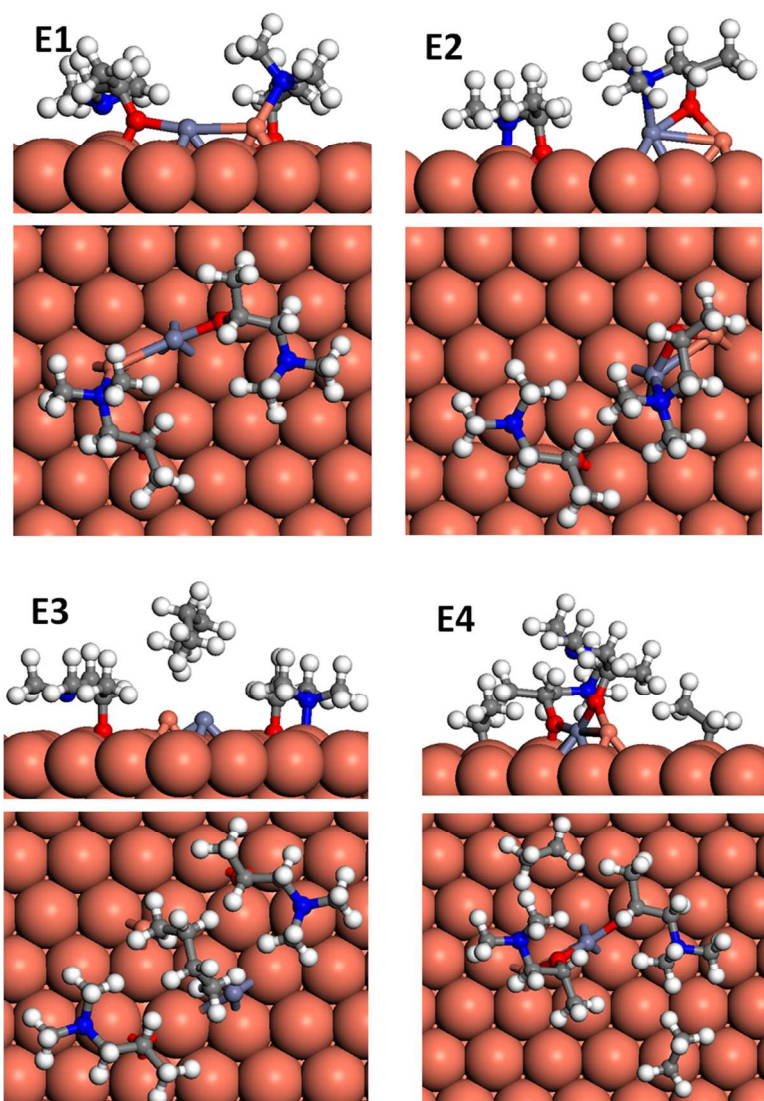
1  
2  
3 to render the  $\text{Zn}(\text{dmap})_2$  by-product under mild ALD conditions. The activation energy for  
4  
5  $\text{D1} \rightarrow \text{E2}$  is twice greater than that of  $\text{D1} \rightarrow \text{E1}$ . This is because the dmap ligand in the  $\text{D1} \rightarrow \text{E2}$   
6  
7 process has to move above the Cu-Zn dimer instead of along the smooth Cu(111) surface, which  
8  
9 makes the diffusion of dmap more difficult. In the E2 structure, the O atom in Cu(dmap) attaches  
10  
11 to the Zn atom and a trimer of Zn-Cu-O is formed.  
12  
13

14  
15 We investigated whether the two ethyl groups attached to the Cu and Zn in the D2 structure  
16  
17 can combine to yield a butane molecule (E3). The reaction is exothermic ( $\Delta E = -0.68$  eV), but  
18  
19 not as much as other steps that yield butane ( $\Delta E = -2.03$  eV for  $\text{C1} \rightarrow \text{D1}$  and  $\Delta E = -1.49$  eV for  
20  
21  $\text{G2} \rightarrow \text{H2}$ ) and the computed activation energy is high ( $E_a = 0.85$  eV). This suggests that ZnEt  
22  
23 resists loss of the Et ligands. The Cu to Zn distance is 4.47 Å and the distances between O atoms  
24  
25 in the dmap ligand and the Zn atom are 4.22 Å and 4.69 Å in configuration E3.  
26  
27

28  
29 Because the D2 configuration has a complex surface structure consisting of two dmap, CuEt  
30  
31 and ZnEt fragments, we check the viability of parasitic reactions to form (dmap)CuEt and  
32  
33 (dmap)Et intermediates. Although the formation of the (dmap)CuEt intermediate adsorbate is  
34  
35 found to be possible with the  $E_a = 0.44$  eV and  $\Delta E = +0.16$  eV, the desorption of that molecule is  
36  
37 unlikely as it needs an activation energy  $E_a$  of 2.25 eV (Table S1, Supporting information). Since  
38  
39 formation of this (dmap)CuEt adsorbate is endothermic ( $\Delta E = +0.16$  eV), it is likely that the  
40  
41 reverse reaction from this intermediate product to CuEt, Cu(dmap) and ZnEt in configuration D2  
42  
43 may take place with the reverse activation barrier  $E_a = 0.28$  eV. This means that (dmap)CuEt is  
44  
45 transient and decomposes, returning to the D2 configuration. We also found that the formation  
46  
47 and desorption of (dmap)Et is not accessible because it also faces a high barrier ( $E_a = 1.82$  eV,  
48  
49 Table S1 Supporting Information). This supports the assumption in Figure 1b about the by-  
50  
51  
52  
53  
54  
55  
56  
57  
58  
59  
60

1  
2  
3 products of ALD. Therefore, butane formation ( $D2 \rightarrow E3$ ) is the most likely step from the  $D2$   
4 configuration, albeit kinetically hindered.  
5  
6

7  
8 For configuration  $E4$ , two  $dmap$  ligands from  $D3$  diffuse toward the  $Zn$  atom to form the  
9  $Zn(dmap)_2$  molecule, with an activation energy of 0.33 eV and  $\Delta E = +0.20$  eV. Through the  
10 endothermic reaction pathway  $B1 \rightarrow C1 \rightarrow D3 \rightarrow E4$ , the  $Zn(dmap)_2$  may be formed as the ethyl  
11 groups are donated to the copper surface.  
12  
13  
14  
15  
16  
17



54  
55 Figure 8. step E: ligand diffusion.  $E1$  and  $E2$  are reaction products of  $D1$ .  $E3$  and  $E4$  are the  
56  
57 reaction products of  $D2$  and  $D3$ , respectively.  
58  
59  
60

1  
2  
3 **F: Ligand re-ordering (step 1a & 2a).** Although dmap ligands have diffused toward the Zn  
4 atom in the previous step, the Zn(dmap)<sub>2</sub> molecule is not yet formed because the Zn atom is not  
5 coordinated with both the O and N atoms in the dmap ligands. Therefore after the dmap ligands  
6 have diffused towards the Zn atom, they may re-order their atomic positions to form a Zn(dmap)<sub>2</sub>  
7 molecule. Figure 9 shows the re-ordered dmap ligands around the Zn atom.  
8  
9

10  
11  
12  
13  
14  
15 The E1 → F1 reaction consists of the migration of dmap from adatom Cu to the Zn atom and  
16 needs activation of 0.44 eV. The reaction is endothermic with  $\Delta E = 0.37$  eV. As we can see from  
17 the F1 configuration, the Zn(dmap)<sub>2</sub> structure is still deformed and the N–Zn distances are 1.9 Å  
18 and 3.8 Å, respectively.  
19

20  
21  
22  
23  
24  
25 The reaction E2 → F2 involves the scission of the Zn–Cu bond and re-ordering of dmap  
26 ligands so that the O atom in dmap forms a bond with the Zn atom, which needs  $E_a$  of 0.62 eV.  
27 In this case, the long O–Zn distance is 4.2 Å. Thus, to form the F2 configuration, the ligands  
28 have to move further than E1 → F1 to form the Zn(dmap)<sub>2</sub> molecule.  
29

30  
31  
32  
33  
34  
35 The F3 configuration is obtained after removing the butane molecule in the E3 structure and  
36 optimizing the geometry. The O atoms in the dmap ligands are attached to the Zn atom in the F3  
37 configuration. The process E3 → F3 is slightly endothermic with a reaction energy of +0.35 eV,  
38 and an activation barrier of 0.71 eV.  
39

40  
41  
42  
43  
44  
45 In the F4 configuration, the Zn(dmap)<sub>2</sub> by-product molecule is formed in the presence of two  
46 ethyl groups on the surface. Obtaining F4 from E4 needs an  $E_a$  of 0.56 eV and  $\Delta E$  of +0.30 eV.  
47 Comparing F4 with the F1, F2 and F3 structures, we can see that the F4 adsorbate is the closest  
48 in structure to Zn(dmap)<sub>2</sub>, as is evident from the formation of all Zn – O (1.97 Å) and Zn – N  
49 (2.29 Å) bonds. We note that the surface in F4 is more crowded with the presence of Et groups  
50 and this may facilitate the formation of Zn(dmap)<sub>2</sub>.  
51  
52  
53  
54  
55  
56  
57  
58  
59  
60

1  
2  
3 Overall, during the E → F process, the dmap ligands re-order around Zn to form the  
4 Zn(dmap)<sub>2</sub> molecule prior to desorption (step G). However, this process is endothermic with  
5  
6 reaction energies of +0.3 to +0.4 eV and needs high activation energies ranging between 0.4 and  
7  
8 0.8 eV. This suggests that diffusion of dmap across the surface is slow and that perfect packing  
9  
10 of dmap ligands may not be achieved over the timescale of the Cu(dmap)<sub>2</sub> pulse. Small sections  
11  
12 of bare Cu may therefore still exist on the surface at the end of step 1b.  
13  
14  
15  
16

17  
18 The energetics of E → F also indicate that the overall formation of Zn(dmap)<sub>2</sub> is a relatively  
19  
20 slow process. The reverse reactions F → E will therefore happen with the higher reaction rate  
21  
22 than E → F. This may result in residual dmap ligands blocking surface sites at the end of the  
23  
24 Et<sub>2</sub>Zn pulse, which in turn will block further adsorption and reduce the overall ALD growth rate.  
25  
26  
27 At low temperature therefore, some of the dmap ligands may not be desorbed and may remain  
28  
29 inside the deposited Cu thin film in some form. This may also explain C and O incorporation into  
30  
31 Cu thin films which is observed in experiment below temperatures of 100 °C.<sup>20</sup> However, our  
32  
33 calculations do not explain why C and O impurities are also detected experimentally at  
34  
35 temperatures above 130 °C. In addition, residual Zn cations may be reduced to Zn metal and  
36  
37 incorporated as an impurity. This too was observed in growth experiments (8 – 15 % Zn impurity  
38  
39 at 120 – 150 °C).<sup>20</sup>  
40  
41  
42  
43  
44  
45  
46  
47  
48  
49  
50  
51  
52  
53  
54  
55  
56  
57  
58  
59  
60



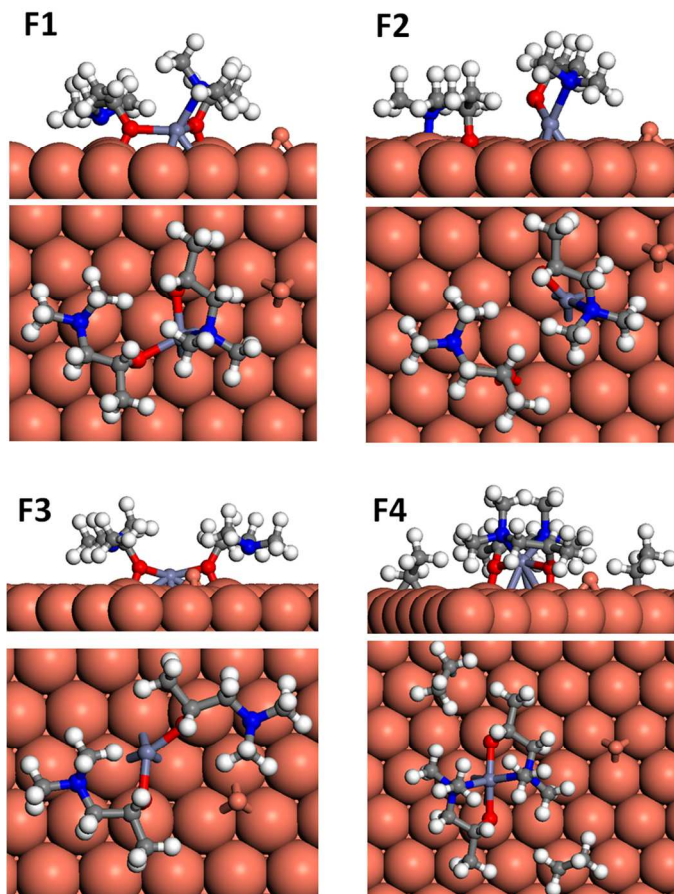


Figure 9. Step F: ligand re-ordering. Configuration F1 and F2 are reaction products of E1 and E2, respectively. F3 configuration is obtained after removing the butane molecule in E3. F4 is obtained from E3.

**G:  $\text{Zn(dmap)}_2$  or  $\text{Cu(Et)}_2$  formation at the surface (step 1a & 2a).** After ligand diffusion and ligand re-ordering steps, a  $\text{Zn(dmap)}_2$  molecule can be formed from these re-ordered ligands. In the F1, F2 and F3 configurations, the O atoms of dmap ligands attach to the Zn atom and only the spatial arrangements of dmap and  $\text{Zn(dmap)}$  fragments differ slightly. Thus these three structures can re-order so as to yield a single configuration G1, as shown in Figure 10. The activation energy for achieving G1 from F1 (0.78 eV) is approximately twice greater than that of achieving G1 from F3 (0.32 eV). The process  $\text{F2} \rightarrow \text{G1}$  only needs an activation energy of 0.15

1  
2  
3 eV because the Zn atom is already coordinated to the ligand in the F2 configuration. The two  
4  
5 processes of Zn(dmap)<sub>2</sub> formation from F1 and F2 are endothermic with reaction energies of  
6  
7 +0.43 eV and +0.05 eV, respectively. In configuration G1, Zn(dmap)<sub>2</sub> is not fully shaped, as one  
8  
9 of the Cu–N distances is greater than its gas phase bond length by 1.6 Å. By comparing the  
10  
11 Cu(dmap)<sub>2</sub> chemisorbed on Cu(111) with configuration G1, we can find that it has some  
12  
13 common features: O–Zn–O atoms form bonds with the surface Cu atoms, and N-containing  
14  
15 parts of the ligand are distorted. This indicates that G1 is indeed the chemisorbed Zn(dmap)<sub>2</sub> on  
16  
17 the Cu(111) surface. Next in the proposed mechanism, this chemisorbed Zn(dmap)<sub>2</sub> molecule  
18  
19 should desorb from the surface (step H).  
20  
21  
22  
23  
24

25 The ethyl groups or the deposited Cu adatom migrate to form a an adsorbed Cu(Et)<sub>2</sub> unit in  
26  
27 configuration G2, which follows the desorption of the Zn(dmap)<sub>2</sub> molecule in configuration F4.  
28  
29 We found that formation of butane from ethyl groups on the smooth surface is not kinetically  
30  
31 favourable, because it needs an activation energy of 0.99 eV (Table S1 in Supporting  
32  
33 Information). However in G2, the deposited Cu adatom can diffuse on the surface with a  
34  
35 relatively small energy cost ( $E_a = 0.02$  eV from one hollow site to the neighbouring hollow site),  
36  
37 and so we moved the deposited Cu adatom between the two ethyl groups to form the Cu(Et)<sub>2</sub>  
38  
39 intermediate. The activation barrier to form the Cu(Et)<sub>2</sub> adsorbate in configuration G2 from F4  
40  
41 (after removing the Zn(dmap)<sub>2</sub> molecule and moving the deposited Cu adatom between two ethyl  
42  
43 groups) is 0.49 eV. The reaction is moderately exothermic with reaction energy of -0.38 eV.  
44  
45 Comparison with the barrier for smooth surfaces ( $E_a = 0.99$  eV) indicates that butane formation  
46  
47 is only possible on rough surfaces during the ALD process.  
48  
49  
50  
51  
52  
53  
54  
55  
56  
57  
58  
59  
60

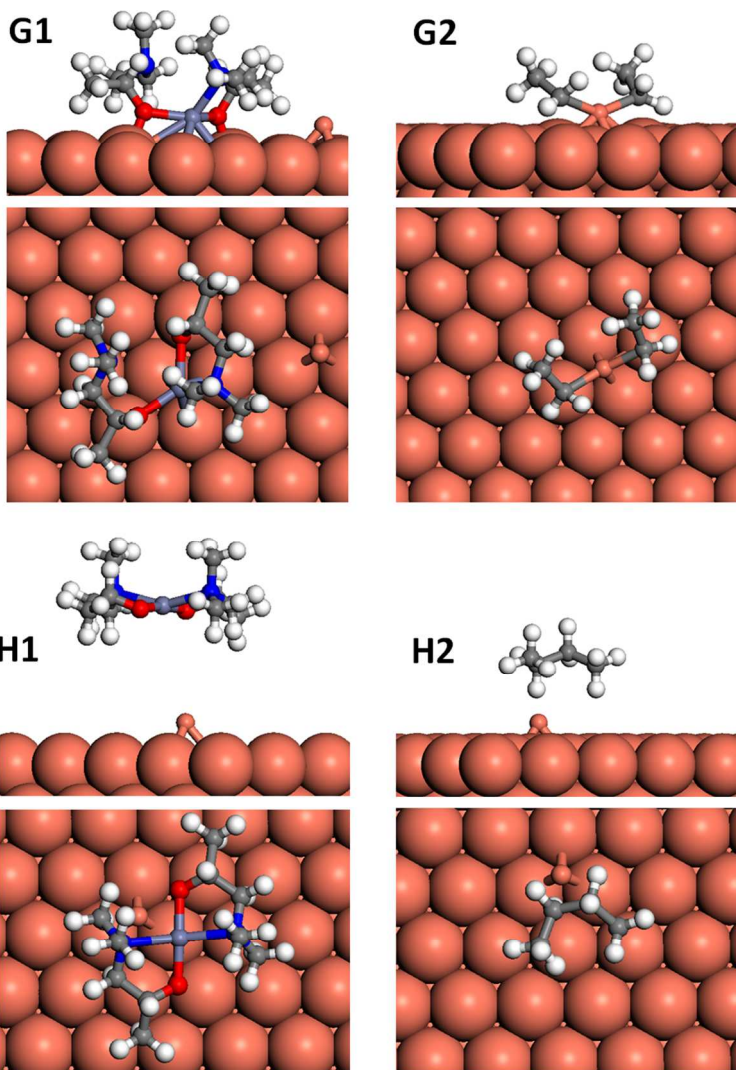


Figure 10. By-product formation (step G) and desorption (step H). G1 which is obtained from F1, F2 and F3 configurations shows the formation of  $\text{Zn}(\text{dmap})_2$ . G2 is obtained after the formation and desorption of the  $\text{Zn}(\text{dmap})_2$  molecule in F4 configuration. As the diffusion of Et groups on bare Cu(111) is not preferred, the  $\text{Cu}(\text{Et})_2$  intermediate product is formed by diffusion of the Cu adatom or Et group. H1 and H2 structures are obtained from G1 and G2, respectively.

**H:  $\text{Zn}(\text{dmap})_2$  or butane desorption (step 1a & 2a).** In the G1 configuration above, dmap ligands re-ordered to form chemisorbed  $\text{Zn}(\text{dmap})_2$  and in H1 this molecule desorbs (Figure 10). It is found that the desorption of  $\text{Zn}(\text{dmap})_2$  from the smooth surface needs an activation energy



1  
2  
3 of 1.34 eV, which makes it not possible under the experimental condition. As the diffusion of  
4 deposited Cu adatom on the Cu(111) surface is nearly barrierless, we moved the Cu near the Zn  
5 atom in G1. The reaction energy  $\Delta E$  of  $\text{Zn}(\text{dmap})_2$  desorption with the help of the Cu adatom is  
6  
7  
8  
9  
10 +0.72 eV and the computed barrier  $E_a$  (0.79 eV) is almost the same, (*i.e.* the adsorption of  
11  
12  $\text{Zn}(\text{dmap})_2$  would be barrierless). The Zn–O and Zn–N bond distances are 1.89 Å and 2.30 Å,  
13  
14 respectively. The desorbed  $\text{Zn}(\text{dmap})_2$  by-product molecule can be purged away to vacate the  
15  
16 surface for new precursor molecules ( $\text{Et}_2\text{Zn}$  in step 2b,  $\text{Cu}(\text{dmap})_2$  in step 1b).  
17  
18  
19

20 In the H2 configuration, which is obtained from configuration G2, the butane molecule desorbs  
21 through the decomposition of the  $\text{Cu}(\text{Et})_2$  molecule into butane, which needs quite a high  
22 activation energy of 0.73 eV. The  $\text{G2} \rightarrow \text{H2}$  process is strongly exothermic with  $\Delta E = -1.49$  eV,  
23  
24 consistent with the other process of butane desorption  $\text{C1} \rightarrow \text{D1}$ . Reduction of the surface as a  
25 whole takes place when two ethyl anions combine and desorb as neutral butane. Once again,  
26  
27 reduction of the surface cations to metallic Cu is achieved in this step by donation of electrons  
28  
29 from ethyl groups as they combine into butane and desorb.  
30  
31  
32  
33  
34  
35

## 36 37 **4. Discussion**

### 38 39 **The reaction mechanism of Cu ALD**

40 The results for step 1b (Section 3.1) show that the  $\text{Cu}(\text{dmap})_2$  pulse seems to involve  
41 dissociative chemisorption of the complex into  $\text{Cu}(\text{dmap})$  and  $\text{dmap}$  (B1 and B2), leaving the  
42  
43 ligands intact. Dissociation within the  $\text{dmap}$  ligand is thermodynamically not preferred (Figure  
44  
45 2), implying that the transmetalation reaction may take place as proposed in Eq. 1. In the original  
46  
47 experimental work,<sup>21</sup> the film thickness increment per cycle for  $\text{Cu}(\text{dmap})_2$  is saturated when the  
48  
49 pulse time exceeds 2 s which allows the full saturation of the surface with the fragments of  
50  
51  
52  
53  
54  
55  
56  
57  
58  
59  
60

1  
2  
3  
4  
5  
6  
7  
8  
9  
10  
11  
12  
13  
14  
15  
16  
17  
18  
19  
20  
21  
22  
23  
24  
25  
26  
27  
28  
29  
30  
31  
32  
33  
34  
35  
36  
37  
38  
39  
40  
41  
42  
43  
44  
45  
46  
47  
48  
49  
50  
51  
52  
53  
54  
55  
56  
57  
58  
59  
60

Cu(dmap)<sub>2</sub>. These thermodynamically stable fragments prevent the further adsorption of precursor.

During step 2a of the second pulse, the Et<sub>2</sub>Zn reducing agent reacts with the Cu(dmap) and dmap fragments and a range of reactions may take place, as shown in Figure 4 and presented in section 3.2. In the experimental work,<sup>21</sup> the pulse time for Et<sub>2</sub>Zn is 0.5 s and Et<sub>2</sub>Zn undergoes self-terminating replacement reaction with the Cu(dmap)<sub>2</sub> adsorbed on the surface. An early formation of the butane molecule (D1) is predicted to be possible just after adsorption of Et<sub>2</sub>Zn; this reaction is extremely exothermic but faces a high kinetic barrier and deposits a Zn atom near dmap and Cu(dmap) fragments. Alternatively, the butane molecule may be formed during the D2 → E3 step after the Et<sub>2</sub>Zn dissociates into ZnEt and Et fragments at the surface.

We also found that parasitic reactions including the formation of (dmap)Cu(Et) and (dmap)(Et) face such high activation barriers that they are not feasible under ALD conditions.

After butane formation and desorption, the dmap ligands diffuse toward the Zn atom and form Zn – O and Zn – N bonds to yield the Zn(dmap)<sub>2</sub> molecule, which finally desorbs from the Cu surface. These reactions (D1 → E1 → F1 → G1, D1 → E2 → F2 → G1 and D2 → E3 → F3 → G1) have activation barriers ranging from 0.3 eV to 0.8 eV, and they are mostly endothermic. This reaction pathway is schematically illustrated in Figure 11a.

For the reaction route involving the D3 structure which has two ethyl groups, dmap and Cu(dmap) fragments attached to the surface relatively sparsely, we introduce a different reaction mechanism based on reaction routes between D3 and H2, which is displayed in Figure 11b. During the C1 → D3 step, the ethyl groups migrate away from Zn to the surface. This provides dmap ligands with access to diffuse toward the under-coordinated Zn atom and re-order

1  
2  
3 to form the  $\text{Zn(dmap)}_2$  molecule during the next steps ( $\text{D3} \rightarrow \text{E4}$  and  $\text{E4} \rightarrow \text{F4}$ ). Desorption of  
4  
5  
6  $\text{Zn(dmap)}_2$  produces a rather bare Cu surface with a low coverage of Et groups.  
7

8 It is found that the formation of butane on the smooth Cu surface is not kinetically accessible,  
9  
10 in contrast to the cooperative role of dmap ligands in step  $\text{C1} \rightarrow \text{D1}$ . The formation of the  
11  
12 intermediate product  $\text{Cu(Et)}_2$  with the help of a migrating Cu atom reduces the activation energy  
13  
14 needed for the formation of butane because this causes the interaction between the Et groups and  
15  
16 the surface to weaken. The butane desorption in the  $\text{F4} \rightarrow \text{G2}$  reaction is again extremely  
17  
18 exothermic, consistent with the step  $\text{C1} \rightarrow \text{D1}$ .  
19  
20  
21

22  
23 The reaction mechanisms shown in Figure 11a and Figure 11b are two possible routes for the  
24  
25 copper ALD reaction proposed in Equation (1). These two different reaction mechanisms stem  
26  
27 from the different coverage of dmap ligands, as we can see from the B1 and B2 configurations in  
28  
29 Figure 3. The reaction mechanism in Figure 11a originates from the surface with relatively dense  
30  
31 ligands and the reaction mechanism in Figure 11b results from the surface less densely saturated  
32  
33 ligands. As we will discuss later, these two types of reaction mechanisms are direct results of  
34  
35 cooperative effects determined by the different coverage of ligands on the surface.  
36  
37  
38

39 As we can see from Figure 4, the reaction energies of most of the ligand diffusion and ligand  
40  
41 re-ordering steps leading to  $\text{Zn(dmap)}_2$  ( $\text{D} \rightarrow \text{G}$ ) are positive and the reaction pathways are uphill  
42  
43 in these stages. This means that the activation barriers for the reverse reactions are smaller than  
44  
45 those of the forward reactions and so the reaction rates of the reverse reactions can be higher  
46  
47 than those of the forward reactions during the ligand diffusion and re-ordering steps.  
48  
49 Nevertheless, desorption of  $\text{Zn(dmap)}_2$  is expected to be irreversible, and this will drive the  
50  
51 equilibrium towards formation of the product (H1). Even so, residual adsorbed dmap (D1) may  
52  
53 block sites against adsorption of  $\text{Cu(dmap)}_2$  in the next ALD cycle. There is recent theoretical<sup>53</sup>  
54  
55  
56  
57  
58  
59  
60

and experimental<sup>54</sup> evidence that ligands persist for multiple cycles in some ALD processes. Slow re-ordering and desorption of the Zn by-product may result in incorporation of Zn into the growing metallic film as an impurity. Indeed 8 - 15 % Zn is detected in the experiment.<sup>20</sup>

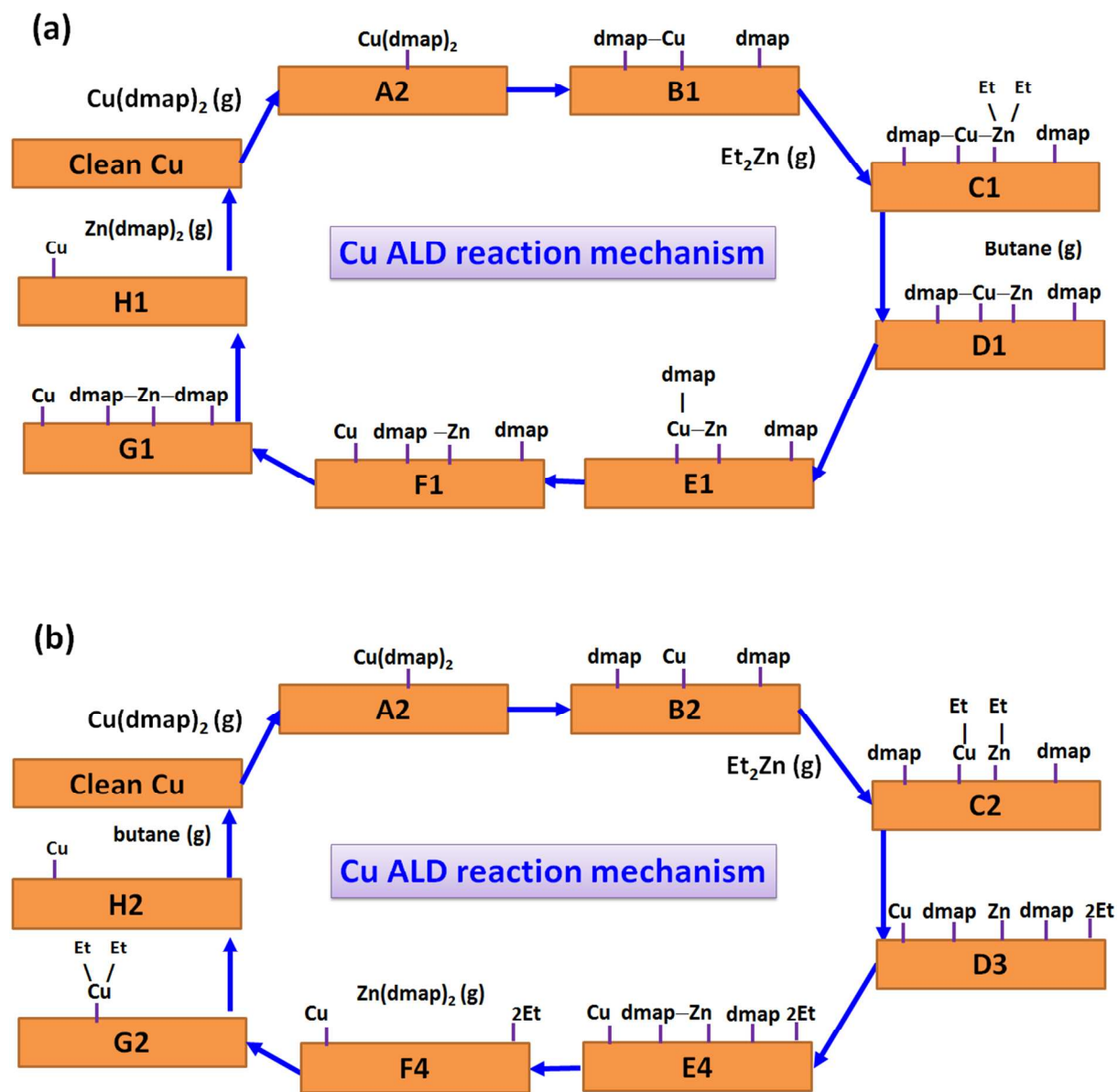


Figure 11. The reaction mechanisms of copper ALD from  $\text{Cu}(\text{dmap})_2$  and  $\text{Et}_2\text{Zn}$ . The capital letters and numbers inside the boxes represent the structures shown in Figure 3 to Figure 10. The mechanism in (a) corresponds to reactions with densely adsorbed precursors in the immediate

1  
2  
3 locality of the Cu atom and the mechanism in (b) corresponds to the reactions of the less densely  
4  
5 adsorbed precursors.  
6  
7

### 8 9 **Estimate of ALD growth rate**

10  
11 Having obtained evidence for the ALD cycle of Figure 1b and likely coverages of ligands at  
12  
13 the end of each step of the cycle, we are now able to estimate the growth rate of Cu in each  
14  
15 cycle. Each Cu<sup>0</sup> atom deposited in step 1a is the result of the reductive elimination of two Et  
16  
17 groups as butane. The reaction is therefore limited by the coverage of Et groups at the end of step  
18  
19 2b, which we conservatively estimate at four Et groups per (6 × 6) simulation cell (section 3.2),  
20  
21 meaning 2 Cu atoms deposited per cell. Further adsorption of Cu(dmap)<sub>2</sub> is possible in step 1b  
22  
23 (for reduction to Cu<sup>0</sup> in step 2a), although we suggest that this is limited by the availability of  
24  
25 sufficiently large segments of bare Cu. Adsorption of one Cu(dmap)<sub>2</sub> molecule per (6 × 6) cell  
26  
27 blocks further adsorption, which gives a reasonable estimate for the amount of Cu deposited in  
28  
29 step 1b. The total amount deposited per cycle is therefore three Cu atoms per (6 × 6) cell, or  
30  
31 3/36 of a monolayer. Since the height of one monolayer of crystalline Cu in the (111) direction  
32  
33 is 2.10 Å in experiment, the predicted growth rate is 3/36 of this, *i.e.* 0.18 Å/cycle. This agrees  
34  
35 remarkably well with the experimental growth rate of 0.2 Å/cycle,<sup>21</sup> which may be fortuitous,  
36  
37 given the many assumptions feeding into the predicted value. Nevertheless, this result illustrates  
38  
39 that the proposed ALD cycle can account for the experimental growth rate.  
40  
41  
42  
43  
44  
45  
46

### 47 **The impact of vdW interaction**

48  
49 In this work, we used pure PBE to calculate the activation barriers and reaction energies for  
50  
51 Cu(dmap)<sub>2</sub> and Et<sub>2</sub>Zn interacting with a Cu surface. In our previous work, we found that the  
52  
53 vdW interaction is an important factor in describing the adsorption of Cu(dmap)<sub>2</sub> on copper  
54  
55 surfaces.<sup>41</sup> Therefore, we now test the impact of vdW interaction on the energetics of the  
56  
57  
58  
59  
60

1  
2  
3 dissociation of one dmap ligand from the  $\text{Cu}(\text{dmap})_2$  molecule adsorbed on  $\text{Cu}(111)$  (A2→B1)  
4 by using the optB88-vdW method. For this reaction, the optB88-vdW method yields an  
5  
6 activation energy  $E_a = 0.55$  eV, which is slightly larger than the PBE value of 0.44 eV, and a  
7  
8 reaction energy of  $\Delta E = -0.10$  eV, which is approximately the same as the PBE calculated  $\Delta E$  of  
9  
10 -0.11 eV. Hu *et al.* used PBE and vdW-DF to calculate the activation barriers for the dissociation  
11  
12 of  $\text{Cu}(\text{acac})_2$  on the  $\text{Cu}(110)$  surface and found that vdW-DF gives a slightly lower activation  
13  
14 barrier than PBE.<sup>38</sup> However, they found that PBE and vdW-DF produce energy profiles with  
15  
16 similar trends for the dissociation of the  $\text{Cu}(\text{acac})_2$  molecule. Slightly different activation  
17  
18 energies but the same trend in energy profiles were also found with vdW-inclusive DFT methods  
19  
20 in other computational works.<sup>55,56</sup> Thus, we argue that inclusion of vdW interaction in DFT may  
21  
22 have a small effect on the values of the activation energies, but that the nature of the reaction  
23  
24 mechanisms described in Figure 11 will probably not be affected.  
25  
26  
27  
28  
29  
30  
31

### 32 **Cooperative role of ligands**

33  
34 It was previously reported that the cooperation between adsorbates plays an important role in the  
35  
36 kinetics of ALD reactions for oxides.<sup>53</sup> Inert adsorbed fragments become reactive once sufficient  
37  
38 numbers of precursors adsorb in their neighborhood. It was not previously known whether  
39  
40 ligand-covered metal surfaces show the same magnitude of cooperative effect as ligand-covered  
41  
42 oxide surfaces. Although we studied the reaction of just one  $\text{Cu}(\text{dmap})_2$  and one  $\text{Et}_2\text{Zn}$  molecule  
43  
44 on a  $2 \text{ nm}^2$  section of  $\text{Cu}(111)$ , we found similar cooperative effects of the inert fragments on  
45  
46 several occasions, as schematically shown in Figure 12.  
47  
48  
49  
50

51 (a) During the butane formation step C1→D1, the activation barrier of 0.78 eV is lowered by  
52  
53 0.21 eV when the dmap and  $\text{Cu}(\text{dmap})$  fragments exist around the adsorbed  $\text{Et}_2\text{Zn}$ . The presence  
54  
55 of these dmap ligands prevents the migration of Et to the Cu surface and enables the formation of  
56  
57  
58  
59  
60

1  
2  
3 butane with a lower activation barrier, explaining the advantage of using a copper metalorganic  
4  
5 compound like  $\text{Cu}(\text{dmap})_2$  in ALD.  
6  
7

8 (b) The formation of the  $\text{Zn}(\text{dmap})_2$  by-product during ligand diffusion and re-ordering steps was  
9  
10 eased by the presence of nearby Et groups (see F4 configuration). The  $\text{E3} \rightarrow \text{F4}$  reaction needs 0.1  
11  
12 – 0.2 eV less activation energy than  $\text{E1} \rightarrow \text{F2}$  and  $\text{E3} \rightarrow \text{F3}$ . Although  $\text{E1} \rightarrow \text{F1}$  requires less  
13  
14 activation energy than  $\text{E3} \rightarrow \text{F4}$ , it faces a higher barrier in the next step. Moreover,  $\text{E3} \rightarrow \text{F4}$   
15  
16 completes formation of  $\text{Zn}(\text{dmap})_2$  in a single step, unlike the other reactions. This implies that  
17  
18 the presence of nearby fragments not only reduces the activation barrier, but it may also speed up  
19  
20 the formation of by-product.  
21  
22  
23  
24

25 (c) We found that butane formation on the bare  $\text{Cu}(111)$  surface needs an activation barrier of  
26  
27 0.99 eV, but that this process can be facilitated with the formation of the  $\text{Cu}(\text{Et})_2$  intermediate  
28  
29 product from a Cu adatom ( $\text{F4} \rightarrow \text{G2} \rightarrow \text{H2}$ ). Butane formation from  $\text{Cu}(\text{Et})_2$  needs 0.5 eV less  
30  
31 activation compared to that without  $\text{Cu}(\text{Et})_2$  on a bare surface. This shows that local roughness  
32  
33 due to newly deposited Cu adatoms also plays a cooperative role in the formation of by-products.  
34  
35  
36  
37  
38  
39  
40  
41  
42  
43  
44  
45  
46  
47  
48  
49  
50  
51  
52  
53  
54  
55  
56  
57  
58  
59  
60

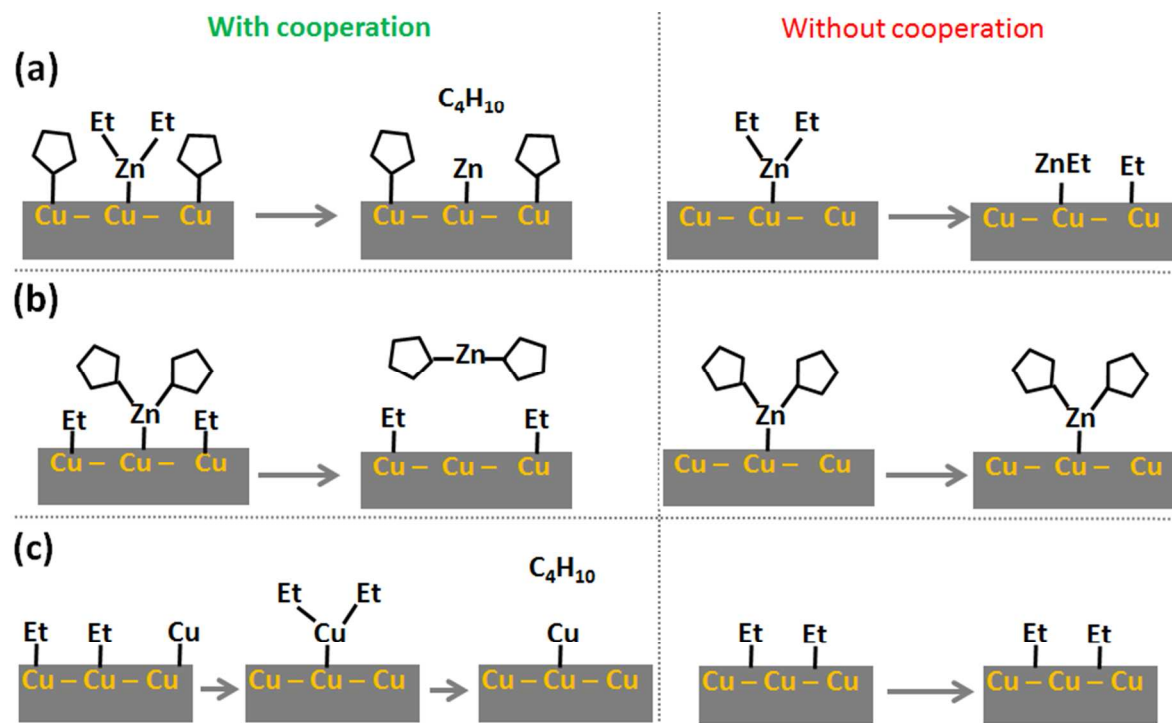


Figure 12. Schematic illustration of several cases of cooperative effects during the ALD of Cu from  $\text{Cu}(\text{dmap})_2$  and  $\text{Et}_2\text{Zn}$ . Pentagonal shapes represent the dmap ligand.

Overall, without the cooperative role of ligands and Cu adatoms, the reaction in Equation 1 would face higher activation barriers and need a higher ALD temperature. This strong dependence of activation energy on proximity of co-adsorbates must also be borne in mind when assessing the quality of our model and accuracy of computed activation energies. If we had modelled the reactions using a smaller cell, e.g.  $\text{Cu}(111) - (5 \times 5)$  or if we had added extra ligands to the surface cell, making the surface more crowded, the activation barriers could have been slightly lower than what is reported in Table 1. However, the qualitative reaction mechanisms proposed in Figure 11 may not be affected.

## 5. Conclusion



1  
2  
3 Atomic layer deposition (ALD) is a promising method for depositing conformal and uniform  
4 thin films of copper for future electronic devices. However, the reaction mechanism and the  
5 surface chemistry of copper ALD have been unclear. In this work, we employ density functional  
6 theory to study the ALD reaction of copper dimethylamino-2-propoxide [Cu(dmap)<sub>2</sub>] and  
7 diethylzinc [Et<sub>2</sub>Zn] based on the seminal paper of Lee *et al.*<sup>21</sup>, computing activation energies and  
8 reaction energies for a range of surface reactions.  
9

10  
11 We found that the chemisorbed Cu(dmap)<sub>2</sub> decomposes through breaking one or both Cu–O on  
12 Cu(111) during the Cu(dmap)<sub>2</sub> pulse. The surface saturates with rather immobile dmap and  
13 Cu(dmap) fragments, which prevents multilayer adsorption of Cu(dmap)<sub>2</sub> precursors, thus  
14 meeting the condition for ALD. The reaction of Et<sub>2</sub>Zn with the dmap and Cu(dmap) fragments  
15 at the surface proceeds via two different reaction routes. The first route starts with butane  
16 formation from the adsorbed Et<sub>2</sub>Zn molecule, aided through the cooperative role of dmap ligands  
17 on the surface. This is followed by the diffusion and reordering of dmap ligands around the Zn  
18 atom to form the Zn(dmap)<sub>2</sub> molecule, which finally desorbs. In the second case, the dmap  
19 ligands diffuse and re-order around the Zn atom. Zn(dmap)<sub>2</sub> is formed and desorbs in the  
20 presence of ethyl groups, which again lower the barriers for these reactions. Subsequently,  
21 butane formation is found not to occur on the bare Cu(111) surface. Instead, the intermediate  
22 reaction product Cu(Et)<sub>2</sub> is formed from the diffusion of adatom Cu on the surface and this  
23 facilitates butane formation and desorption.  
24  
25  
26  
27  
28  
29  
30  
31  
32  
33  
34  
35  
36  
37  
38  
39  
40  
41  
42  
43  
44  
45  
46  
47

48 In general, the butane formation and desorption steps are exothermic while the ligand diffusion  
49 and re-ordering steps are endothermic, which may result in residual dmap ligands blocking  
50 surface sites at the end of the Et<sub>2</sub>Zn pulse, and in residual Zn being reduced and incorporated as  
51  
52  
53  
54  
55  
56  
57  
58  
59  
60

1  
2  
3 an impurity. It is found that the formation and desorption of  $\text{Et}_2\text{Zn}$  and  $\text{Zn}(\text{dmap})_2$  by-products  
4  
5 are facilitated by the presence of nearby ligands (the ‘cooperative effect’).  
6  
7

8 In this transmetalation mechanism, the ALD growth rate is determined both by the saturating  
9  
10 coverage of Et groups at the end of the  $\text{Et}_2\text{Zn}$  pulse (since each contributes one electron towards  
11  
12 reduction of Cu) and by the saturating adsorption of  $\text{Cu}(\text{dmap})_2$  during the Cu pulse. Based on  
13  
14 the rather slow rates of ligand diffusion that we computed, we suggest that saturation is reached  
15  
16 before Et or dmap groups pack perfectly on the surface. We therefore estimate that Cu is  
17  
18 deposited at approximately  $0.18 \text{ \AA}/\text{cycle}$ , which agrees well with experiment.  
19  
20  
21

22 We find that there is competition between alternative surface reactions, both leading to Cu  
23  
24 deposition, and that which reaction mechanism is followed depends on the coverage of the  
25  
26 ligands on the surface. We found that the cooperative role of ligands and Cu adatoms is an  
27  
28 important factor that lowers activation barriers. The method that we used in this study and the  
29  
30 ALD mechanisms that we obtained provide insight into the ALD of copper and other transition  
31  
32 metals.  
33  
34  
35

## 36 ASSOCIATED CONTENT

### 37 Supporting Information

38  
39 The activation and reaction energies of depositing Cu from  $\text{Cu}(\text{dmap})_2$  and  $\text{Et}_2\text{Zn}$  through ALD.  
40  
41 Structures of  $\text{Cu}(\text{dmap})_2$  decomposition on Cu(111) Surface. Reaction energy profiles and  
42  
43 structures of butane formation on Cu(111) surface. This material is available free of charge via  
44  
45 the Internet at <http://pubs.acs.org>.  
46  
47  
48  
49  
50  
51

## 52 AUTHOR INFORMATION

### 53 Corresponding Author

54  
55  
56  
57  
58  
59  
60

\*Phone: +353 21 234 6392. E-mail: [simon.elliott@tyndall.ie](mailto:simon.elliott@tyndall.ie)

## Notes

The authors declare no competing financial interest.

## ACKNOWLEDGEMENTS

We acknowledge support from Science Foundation Ireland (SFI) under the ‘ALDesign’ Project (grant number 09.IN1.I2628). We acknowledge the SFI and Higher Education Authority funded Irish Centre for High Performance Computing (ICHEC) for access and SFI funded computational resources at Tyndall National Institute. Y.M. thanks Dr. Gangotri Dey (George Washington University) for discussions.

## REFERENCES

- (1) Osada, T.; Godwin, M. International Technology Roadmap for Semiconductors <http://www.itrs.net/>.
- (2) Rosenberg, R.; Edelstein, D. C.; Hu, C. K.; Rodbell, K. P. Copper Metallization for High Performance Silicon Technology. *Annu. Rev. Mater. Sci.* **2000**, *30*, 229–262.
- (3) Shacham-Diamand, Y.; Inberg, A.; Sverdlov, Y.; Bogush, V.; Croitoru, N.; Moscovich, H.; Freeman, A. Electroless Processes for Micro- and Nanoelectronics. In *Electrochimica Acta*; 2003; Vol. 48, pp 2987–2996.
- (4) Krisyuk, V.; Aloui, L.; Prud’homme, N.; Sysoev, S.; Senocq, F.; Samélor, D.; Vahlas, C. CVD of Pure Copper Films from Amidinate Precursor. *Electrochem. Solid-State Lett.* **2011**, *14* (3), D26–D29.
- (5) Törndahl, T.; Ottosson, M.; Carlsson, J.-O. Growth of Copper Metal by Atomic Layer Deposition Using copper(I) Chloride, Water and Hydrogen as Precursors. *Thin Solid Films* **2004**, *458* (1-2), 129–136.
- (6) Knisley, T. J.; Ariyasena, T. C.; Sajavaara, T.; Saly, M. J.; Winter, C. H. Low Temperature Growth of High Purity, Low Resistivity Copper Films by Atomic Layer Deposition. *Chem. Mater.* **2011**, *23* (20), 4417–4419.
- (7) Coyle, J. P.; Dey, G.; Sirianni, E. R.; Kemell, M. L.; Yap, G. P. A.; Ritala, M.; Leskelä, M.; Elliott, S. D.; Barry, S. T. Deposition of Copper by Plasma-Enhanced Atomic Layer Deposition Using a Novel N-Heterocyclic Carbene Precursor. *Chem. Mater.* **2013**, *25* (7), 1132–1138.

- 1
  - 2
  - 3
  - 4
  - 5
  - 6
  - 7
  - 8
  - 9
  - 10
  - 11
  - 12
  - 13
  - 14
  - 15
  - 16
  - 17
  - 18
  - 19
  - 20
  - 21
  - 22
  - 23
  - 24
  - 25
  - 26
  - 27
  - 28
  - 29
  - 30
  - 31
  - 32
  - 33
  - 34
  - 35
  - 36
  - 37
  - 38
  - 39
  - 40
  - 41
  - 42
  - 43
  - 44
  - 45
  - 46
  - 47
  - 48
  - 49
  - 50
  - 51
  - 52
  - 53
  - 54
  - 55
  - 56
  - 57
  - 58
  - 59
  - 60
- (8) Hagen, D. J.; Povey, I.; Rushworth, S.; Wrench, J. S.; Keeney, L.; Schmidt, M.; Petkov, N.; Barry, S. T.; Coyle, J. P.; Pemble, M. E. Atomic Layer Deposition of Cu Using a Carbene-Stabilized Cu (I) Silylamide. *J. Mater. Chem. C* **2014**, 9205–9214.
- (9) Kalutarage, L. C.; Clendenning, S. B.; Winter, C. H. Low-Temperature Atomic Layer Deposition of Copper Films Using Borane Dimethylamine as the Reducing Co-Reagent. *Chem. Mater.* **2014**, 26 (12), 3731–3738.
- (10) George, S. M. Atomic Layer Deposition: An Overview. *Chem. Rev.* **2010**, 110 (1), 111–131.
- (11) Profijt, H. B.; Potts, S. E.; van de Sanden, M. C. M.; Kessels, W. M. M. Plasma-Assisted Atomic Layer Deposition: Basics, Opportunities, and Challenges. *J. Vac. Sci. Technol. A Vacuum, Surfaces, Film.* **2011**, 29 (5), 50801–50826.
- (12) Miikkulainen, V.; Leskelä, M.; Ritala, M.; Puurunen, R. L. Crystallinity of Inorganic Films Grown by Atomic Layer Deposition: Overview and General Trends. *J. Appl. Phys.* **2013**, 113 (2), 021301.
- (13) Mårtensson, P.; Carlsson, J.-O. Atomic Layer Epitaxy of Copper on Tantalum. *Chem. Vap. Depos.* **1997**, 3 (1), 45–50.
- (14) Niskanen, A.; Rahtu, A.; Sajavaara, T.; Arstila, K.; Ritala, M.; Leskelä, M. Radical-Enhanced Atomic Layer Deposition of Metallic Copper Thin Films. *J. Electrochem. Soc.* **2005**, 152 (1), G25–G28.
- (15) Jezewski, C.; Lanford, W. A.; Wiegand, C. J.; Singh, J. P.; Wang, P.-I.; Senkevich, J. J.; Lu, T.-M. Inductively Coupled Hydrogen Plasma-Assisted Cu ALD on Metallic and Dielectric Surfaces. *J. Electrochem. Soc.* **2005**, 152 (2), C60–C64.
- (16) Li, Z.; Rahtu, A.; Gordon, R. G. Atomic Layer Deposition of Ultrathin Copper Metal Films from a Liquid Copper(I) Amidinate Precursor. *J. Electrochem. Soc.* **2006**, 153 (11), C787–C794.
- (17) Dai, M.; Kwon, J.; Halls, M. D.; Gordon, R. G.; Chabal, Y. J. Surface and Interface Processes during Atomic Layer Deposition of Copper on Silicon Oxide. *Langmuir* **2010**, 26 (6), 3911–3917.
- (18) Gordon, P. G.; Kurek, A.; Barry, S. T. Trends in Copper Precursor Development for CVD and ALD Applications. *ECS J. Solid State Sci. Technol.* **2014**, 4 (1), N3188–N3197.
- (19) Hagen, D. J.; Connolly, J.; Nagle, R.; Povey, I. M.; Rushworth, S.; Carolan, P.; Ma, P.; Pemble, M. E. Plasma Enhanced Atomic Layer Deposition of Copper: A Comparison of Precursors. *Surf. Coatings Technol.* **2013**, 230 (0), 3–12.
- (20) Vidjayacoumar, B.; Emslie, D. J. H.; Clendenning, S. B.; Blackwell, J. M.; Britten, J. F.; Rheingold, A. Investigation of AlMe<sub>3</sub>, BEt<sub>3</sub>, and ZnEt<sub>2</sub> as Co-Reagents for Low-Temperature Copper Metal ALD/Pulsed-CVD. *Chem. Mater.* **2010**, 22 (17), 4844–4853.
- (21) Lee, B. H.; Hwang, J. K.; Nam, J. W.; Lee, S. U.; Kim, J. T.; Koo, S.-M.; Baunemann, A.; Fischer, R. a.; Sung, M. M. Low-Temperature Atomic Layer Deposition of Copper Metal Thin Films: Self-Limiting Surface Reaction of Copper Dimethylamino-2-Propoxide with Diethylzinc. *Angew. Chemie - Int. Ed.* **2009**, 48 (Spp 1119), 4536–4539.

- 1  
2  
3 (22) Hambrock, J.; Schröter, M. K.; Birkner, A.; Wöll, C.; Fischer, R. a. Nano-Brass: Bimetallic Copper/Zinc Colloids by a Nonaqueous Organometallic Route Using [Cu(OCH(Me)CH<sub>2</sub>NMe<sub>2</sub>)<sub>2</sub>] and Et<sub>2</sub>Zn as Precursors. *Chem. Mater.* **2003**, *15* (22), 4217–4222.
- 8 (23) Vidjayacoumar, B.; Emslie, D. J. H.; Blackwell, J. M.; Clendenning, S. B.; Britten, J. F. Solution Reactions of a Bis(pyrrolylaldimate)copper(II) Complex with Peralkyl Zinc, Aluminum, and Boron Reagents: Investigation of the Pathways Responsible for Copper Metal Deposition. *Chem. Mater.* **2010**, *22* (17), 4854–4866.
- 14 (24) Dey, G.; Wrench, J. S.; Hagen, D. J.; Keeney, L.; Elliott, S. D. Quantum Chemical and Solution Phase Evaluation of Metallocenes as Reducing Agents for the Prospective Atomic Layer Deposition of Copper. *Dalt. Trans.* **2015**, *44* (22), 10188–10199.
- 18 (25) Guo, Z.; Li, H.; Chen, Q.; Sang, L.; Yang, L.; Liu, Z.; Wang, X. Low-Temperature Atomic Layer Deposition of High Purity, Smooth, Low Resistivity Copper Films by Using Amidinate Precursor and Hydrogen Plasma. *Chem. Mater.* **2015**, *27* (17), 5988–5996.
- 22 (26) Elliott, S. D. Atomic-Scale Simulation of ALD Chemistry. *Semicond. Sci. Technol.* **2012**, *27* (7), 074008.
- 25 (27) Elliott, S. D.; Greer, J. C. Simulating the Atomic Layer Deposition of Alumina from First Principles. *J. Mater. Chem.* **2004**, *14* (21), 3246–3250.
- 28 (28) Nolan, M.; Elliott, S. D. Competing Mechanisms in Atomic Layer Deposition of Er<sub>2</sub>O<sub>3</sub> versus La<sub>2</sub>O<sub>3</sub> from Cyclopentadienyl Precursors. *Chem. Mater.* **2010**, *22* (1), 117–129.
- 31 (29) Shirazi, M.; Elliott, S. D. Multiple Proton Diffusion and Film Densification in Atomic Layer Deposition Modeled by Density Functional Theory. *Chem. Mater.* **2013**, *25* (6), 878–889.
- 35 (30) Dey, G.; Elliott, S. D. Mechanism for the Atomic Layer Deposition of Copper Using Diethylzinc as the Reducing Agent: A Density Functional Theory Study Using Gas-Phase Molecules as a Model. *J. Phys. Chem. A* **2012**, *116* (35), 8893–8901.
- 40 (31) Phung, Q. M.; Vancoillie, S.; Pourtois, G.; Swerts, J.; Pierloot, K.; Delabie, A. Atomic Layer Deposition of Ruthenium on a Titanium Nitride Surface: A Density Functional Theory Study. *J. Phys. Chem. C* **2013**, *117* (38), 19442–19453.
- 44 (32) Elliott, S. D.; Dey, G.; Maimaiti, Y.; Ablat, H.; Filatova, E. A.; Fomengia, G. N. Modeling Mechanism and Growth Reactions for New Nanofabrication Processes by Atomic Layer Deposition. *Adv. Mater.* **2015**, 5367–5380.
- 48 (33) Jiang, X.; Wang, H.; Qi, J.; Willis, B. G. In-Situ Spectroscopic Ellipsometry Study of Copper Selective-Area Atomic Layer Deposition on Palladium. *J. Vac. Sci. Technol. A Vacuum, Surfaces, Film.* **2014**, *32* (4), 041513.
- 52 (34) Minjauw, M. M.; Dendooven, J.; Capon, B.; Schaeckers, M.; Detavernier, C. Atomic Layer Deposition of Ruthenium at 100 °C Using the RuO<sub>4</sub>-Precursor and H<sub>2</sub>. *J. Mater. Chem. C* **2015**, *3* (1), 132–137.
- 56 (35) Dey, G.; Elliott, S. Copper(I) Carbene Hydride Complexes Acting Both as Reducing Agent and Precursor for Cu ALD: A Study through Density Functional Theory. *Theor.*

- 1  
2  
3  
4  
5  
6  
7  
8  
9  
10  
11  
12  
13  
14  
15  
16  
17  
18  
19  
20  
21  
22  
23  
24  
25  
26  
27  
28  
29  
30  
31  
32  
33  
34  
35  
36  
37  
38  
39  
40  
41  
42  
43  
44  
45  
46  
47  
48  
49  
50  
51  
52  
53  
54  
55  
56  
57  
58  
59  
60
- Chem. Acc.* **2013**, *133* (1), 1–7.
- (36) Dey, G.; Elliott, S. D. Quantum Chemical Study of the Effect of Precursor Stereochemistry on Dissociative Chemisorption and Surface Redox Reactions During the Atomic Layer Deposition of the Transition Metal Copper. *J. Phys. Chem. C* **2015**, *119* (11), 5914–5927.
- (37) Hu, X.; Schuster, J.; Schulz, S. E.; Gessner, T. Simulation of ALD Chemistry of (nBu<sub>3</sub>P)Cu(acac) and Cu(acac)<sub>2</sub> Precursors on Ta(110) Surface. *Microelectron. Eng.* **2015**, *137*, 23–31.
- (38) Hu, X.; Schuster, J.; Schulz, S. E.; Gessner, T. Surface Chemistry of Copper Metal and Copper Oxide Atomic Layer Deposition from copper(II) Acetylacetonate: A Combined First-Principles and Reactive Molecular Dynamics Study. *Phys. Chem. Chem. Phys.* **2015**, *17* (40), 26892–26902.
- (39) Ma, Q.; Guo, H.; Gordon, R. G.; Zaera, F. Surface Chemistry of Copper(I) Acetamidates in Connection with Atomic Layer Deposition (ALD) Processes. *Chem. Mater.* **2011**, *23* (14), 3325–3334.
- (40) Maimaiti, Y.; Nolan, M.; Elliott, S. D. Reduction Mechanisms of the CuO(111) Surface through Surface Oxygen Vacancy Formation and Hydrogen Adsorption. *Phys. Chem. Chem. Phys.* **2014**, *16*, 3036–3046.
- (41) Maimaiti, Y.; Elliott, S. D. Precursor Adsorption on Copper Surfaces as the First Step during the Deposition of Copper: A Density Functional Study with van Der Waals Correction. *J. Phys. Chem. C* **2015**, *119* (17), 9375–9385.
- (42) Maimaiti, Y. Computational Study of the Growth of Copper Thin Films by Atomic Layer Deposition, University College Cork, 2015.
- (43) Elliott, S. D.; Scarel, G.; Wiemer, C.; Fanciulli, M.; Pavia, G. Ozone-Based Atomic Layer Deposition of Alumina from TMA: Growth, Morphology, and Reaction Mechanism. *Chem. Mater.* **2006**, *18* (16), 3764–3773.
- (44) Weckman, T.; Laasonen, K. First Principles Study of the Atomic Layer Deposition of Alumina by TMA/H<sub>2</sub>O-Process. *Phys. Chem. Chem. Phys.* **2015**, *17* (1), 17322–17334.
- (45) Kresse, G.; Hafner, J. Ab Initio Molecular-Dynamics Simulation of the Liquid-Metal-Amorphous-Semiconductor Transition in Germanium. *Phys Rev B Condens Matter* **1994**, *49* (20), 14251–14269.
- (46) Kresse, G.; Furthmüller, J. Efficiency of Ab-Initio Total Energy Calculations for Metals and Semiconductors Using a Plane-Wave Basis Set. *Comput. Mater. Sci.* **1996**, *6* (1), 15–50.
- (47) Blochl, P. E. Projector Augmented-Wave Method. *Phys. Rev. B* **1994**, *50* (24), 17953–17979.
- (48) Perdew, J. P.; Burke, K.; Ernzerhof, M. Generalized Gradient Approximation Made Simple. *Phys. Rev. Lett.* **1996**, *77* (18), 3865–3868.
- (49) Dion, M.; Rydberg, H.; Schroder, E.; Langreth, D. C.; Lundqvist, B. I. Van Der Waals

- 1  
2  
3 Density Functional for General Geometries. *Phys. Rev. Lett.* **2004**, 92 (24), 246401.  
4  
5 (50) Klimeš, J.; Michaelides, A. Perspective: Advances and Challenges in Treating van Der  
6 Waals Dispersion Forces in Density Functional Theory. *J. Chem. Phys.* **2012**, 137 (12),  
7 120901–120912.  
8  
9 (51) Henkelman, G.; Uberuaga, B. P.; Jonsson, H. A Climbing Image Nudged Elastic Band  
10 Method for Finding Saddle Points and Minimum Energy Paths. *J. Chem. Phys.* **2000**, 113  
11 (22), 9901–9904.  
12  
13 (52) Henkelman, G.; Jónsson, H. Improved Tangent Estimate in the Nudged Elastic Band  
14 Method for Finding Minimum Energy Paths and Saddle Points. *J. Chem. Phys.* **2000**, 113  
15 (22), 9978.  
16  
17 (53) Shirazi, M.; Elliott, S. D. Cooperation between Adsorbates Accounts for the Activation of  
18 Atomic Layer Deposition Reactions. *Nanoscale* **2015**, 7 (14), 6311–6318.  
19  
20 (54) Vandalon, V.; Kessels, W. M. M. What Is Limiting Low-Temperature Atomic Layer  
21 Deposition of Al<sub>2</sub>O<sub>3</sub>? A Vibrational Sum-Frequency Generation Study. *Appl. Phys. Lett.*  
22 **2016**, 108 (1), 011607–011611.  
23  
24 (55) Liu, W.; Savara, A.; Ren, X.; Ludwig, W.; Dostert, K.-H.; Schauermaun, S.; Tkatchenko,  
25 A.; Freund, H.-J.; Scheffler, M. Toward Low-Temperature Dehydrogenation Catalysis:  
26 Isophorone Adsorbed on Pd(111). *J. Phys. Chem. Lett.* **2012**, 3 (5), 582–586.  
27  
28 (56) Tillotson, M. J.; Brett, P. M.; Bennett, R. a.; Grau-Crespo, R. Adsorption of Organic  
29 Molecules at the TiO<sub>2</sub>(110) Surface: The Effect of van Der Waals Interactions. *Surf. Sci.*  
30 **2015**, 632, 142–153.  
31  
32  
33  
34  
35  
36  
37  
38  
39  
40  
41  
42  
43  
44  
45  
46  
47  
48  
49  
50  
51  
52  
53  
54  
55  
56  
57  
58  
59  
60

## Table of Contents Graphic

